The Optical Parametric Oscillator: Saturating Blow-Up in the large detuning limit.

by

J F Williams
B.Sc., Simon Fraser University, 1998.

A THESIS SUBMITTED IN PARTIAL FULFILLMENT
OF THE REQUIREMENTS FOR THE DEGREE OF
MASTER OF SCIENCE
in the Department
of
Mathematics & Statistics.

SIMON FRASER UNIVERSITY
August 2000

Abstract.

The optical parametric oscillator (OPO) is a source of tunable laser radiation which possesses a rich array of pattern formation capabilities and has applications to optical communication and information processing. In this thesis, I derive the OPO equations - a coupled pair of nonlinear dispersive partial differential equations - which model the patterns generated by this device. In the literature, the large detuning limit of the full OPO system has been modeled by the parametrically forced nonlinear Schrodinger equation (PNLS). The OPO and PNLS are in good agreement in one space dimension, however, in two space dimensions the PNLS fails to capture significant dynamics of the full OPO. Specifically, the PNLS possesses L^∞ blow-up solutions akin to those of the nonlinear Schrodinger equation (NLS) while blow-up is arrested by higher order terms in the OPO.

The limit of large pump detuning in OPO is singular, and I propose that the pump field is slaved to the signal field, permitting a reduction of OPO to a single equation. The relation between pump and signal fields is complicated but admits a natural family of approximations; the leading order approximation recovers the PNLS equation. The second order approximation includes higher order nonlinear and dispersive terms, and the resulting equation - the saturating parametrically forced nonlinear Schrodinger equation (SPNLS) - is a more faithful model of the full OPO. Via detailed numerical analysis using moving mesh methods, I demonstrate that the PNLS exhibits an L^∞ blow-up in two space dimensions. However the OPO and SPNLS share a complex dynamic in which the rapid growth in L^∞ norm saturates and leads to decaying temporal oscillations and dispersive radiation. Following Fibich and Papanicolau, I employ intermediate asymptotics to show the saturation phenomena in the SPNLS is governed by two coupled nonlinear ordinary differential equations which permit an identification of the saturation mechanism.

Acknowledgments.

Many thanks to Keith Promislow for guidance, support and friendship while working on this and other problems. I leave a better person for having known him.

Contents

List of Figures

Chapter 1

Introduction

1.1 Historical Development

Interest in the nonlinear effects in optical crystals predates the study of fiber optics. In 1961, one year after the first successful demonstration of a working laser, [1], second-harmonic generation was discovered in optical crystals. It was not until 1966 that optical fibers were suggested as a mechanism for optical transmission. In 1973, in the ground-breaking work of Hasegawa and Tappert, [2], it was shown that the propagation of an optical pulse in a fiber optic cable is governed by the much bally-hooed nonlinear Schrodinger equation (NLS). However, it was not until 1980 that pulse propagation in optical fibers was demonstrated experimentally [3]. In the last 15 years, these three technologies: laser, optical crystal, and fiber optic cable have been brought together to form optical parametric devices such as the optical parametric oscillator (OPO) and the optical fiber parametric amplifier.

1.2 Physical Description

The optical parametric oscillator is a device for tuning laser frequencies. Light at one frequency is directed into a cavity - a piece of crystal bounded by mirrors - and through interactions with the crystal the frequency is changed. In the down-conversion case, one photon with frequency ω_1 is converted into photons with frequencies ω_2, ω_3 satisfying $\omega_2 + \omega_3 = \omega_1$. In the degenerate case, which we address in this thesis, $\omega_2 = \omega_3 = \frac{\omega_1}{2}$. In the case of up-conversion, two photons of lower frequency combine to form one of higher frequency. Non-linear effects of crystals were first observed in the case of up-conversion, also called second-harmonic generation. The devices and models for up and down conversion are quite similar; the difference lies in the frequency of the pump. A schematic

of the device is presented in figure (1.1).

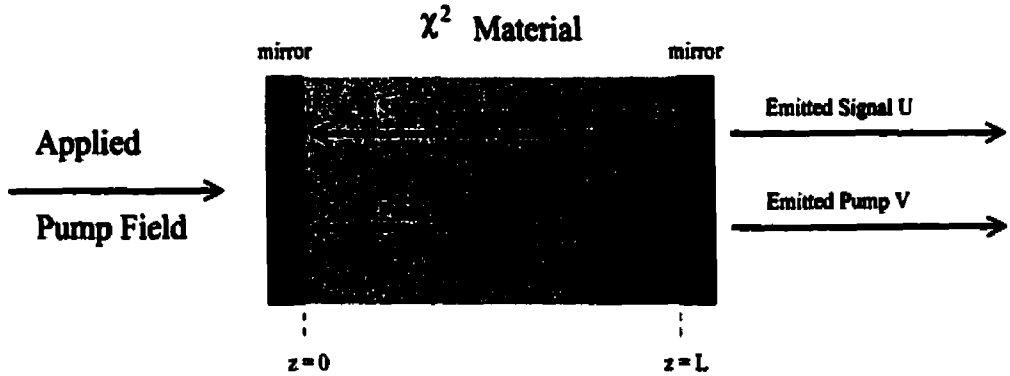

Figure 1.1: Schematic of the OPO

1.3 Derivation of the OPO equations

We derive the model equations from the Maxwell equations under the assumption that the electric fields are nearly mono-chromatic modulated plane waves. It is interesting to note that while this is the accepted leading order model for a doubly-degenerate optical parametric oscillator [4, 5, 6, 7, 8, 9, 13], a complete derivation appears nowhere in the literature.

We begin with Maxwell's equations for the propagation of an electro-magnetic field in a dielectric medium free of currents and point charges

$$\begin{aligned} \nabla \cdot \mathbf{D} &= 0 \\ \nabla \cdot \mathbf{B} &= 0 \\ \nabla \times \mathbf{E} &= -\frac{\partial \mathbf{B}}{\partial t} \\ \nabla \times \mathbf{H} &= \frac{\partial \mathbf{D}}{\partial t}. \end{aligned} \tag{1.1}$$

Here $\mathbf{B}$ and $\mathbf{D}$ are the magnetic and electric inductions respectively and $\mathbf{H}$ and $\mathbf{E}$ are the magnetic and electric fields. We also have the constitutive relations

$$\begin{aligned} \mathbf{B} &= \mu \mathbf{H} \\ \mathbf{D} &= \epsilon_0 \mathbf{E} + \mathbf{P} \end{aligned} \tag{1.2}$$

The permittivity of free space, ϵ_0, and the magnetic permeability, μ, are related to the speed of light in free space, c, by $\epsilon_0 \mu = c^{-2}$. The polarization, $\mathbf{P}$, describes the macroscopic effect of the

displacement of bound electrons in the presence of an applied electric field. Recognizing that for an arbitrary vector in 3 dimensions, $\nabla \times (\nabla \times \mathbf{V}) = -\nabla^2\mathbf{V} + \nabla(\nabla \cdot \mathbf{V})$, and that $\mathbf{E}$ is divergence free, $\nabla \cdot \mathbf{E} = 0$, we can rewrite (1.1) - (1.2) as a wave equation

$$c^2\nabla^2\mathbf{E} - \frac{\partial^2\mathbf{E}}{\partial t^2} = \frac{1}{\epsilon_0}\frac{\partial^2\mathbf{P}}{\partial t^2}. \tag{1.3}$$

Because we are studying the degenerate case, the electric field has two distinct components: $\mathbf{E}_p$ for the pump field and $\mathbf{E}_s$ for the signal field. The frequencies ω_p and ω_s satisfy $\omega_p = 2\omega_s = 2\omega$. Under the approximation of a linear dispersion relation (see equation (1.8)) and assuming there is no phase-mismatch in the direction of propagation we have relations for the the wave numbers k_p and k_s, $k_p = 2k_s = 2k$. Formally, our assumption that the field takes the form of two nearly mono-chromatic modulated plane waves allows us to write

$$\begin{aligned} \mathbf{E}_p &= E_p(\mathbf{r},t)e^{2i(kz-\omega t)}\mathbf{k} \\ \mathbf{P}_p &= P_p(\mathbf{r},t)e^{2i(kz-\omega t)}\mathbf{k} \\ \mathbf{E}_s &= E_s(\mathbf{r},t)e^{i(kz-\omega t)}\mathbf{k} \\ \mathbf{P}_s &= P_s(\mathbf{r},t)e^{i(kz-\omega t)}\mathbf{k}. \end{aligned} \tag{1.4}$$

Here $\mathbf{k}$ is the unit vector in the z-direction, $\mathbf{r}$ is the co-ordinate in the transverse plane, t is time, $\mathbf{E}$ and $\mathbf{P}$ are the electric and polarization vectors respectively and E and P are the electric and polarization envelopes. It is noted in [10] that from experimental evidence in a $\chi^{(2)}$ material with N interacting electric fields, $\mathbf{E}_j$ $j = 1..N$, an appropriate expansion for $\mathbf{P}_j$, the j-th polarization is $\mathbf{P}_j = P_j\phi_j\mathbf{k}$ where

$$P_j\phi_j = \epsilon_0\chi_j^{(1)}\phi_j + \sum_{m,n=1}^{N} \chi_{jmn}^{(2a)} E_m E_n \phi_m \phi_n + \sum_{m,n=1}^{N} \chi_{jmn}^{(2b)} E_m E_n^* \phi_m \phi_n^* \tag{1.5}$$

with the phases given by

$$\phi_j = e^{i(k_j z - \omega_j t)}.$$

The tensors χ^1 and χ^2 denote the first and second order susceptibilities respectively, which measure the magnitude of the nonlinear response of the medium at different frequencies. Higher order terms, eg. the contribution from the χ^3 tensor, have been neglected because for the materials in question $|\chi^2| \gg |\chi^3|$. The polarization is expressed as a convolution over time of the susceptibilities and the electric field, however, assuming that the response of the material is nearly instantaneous this relation reduces to equation (1.5). With this general constitutive relation between E_j and P_j, we can return to (1.3) and (1.4) to derive the governing equations for the envelopes E_p and E_s.

The near monochromaticity assumption implies the phases of the signal and pump envelopes have the form

$$\phi_s = e^{i(kz-\omega t)} \qquad \text{and} \qquad \phi_p = e^{2i(kz-\omega t)}.$$

These functions enjoy the properties

$$\phi_s^2 = \phi_p \qquad \text{and} \qquad \phi_p \phi_s^* = \phi_s.$$

Taking $1 = s$, $2 = p$ and $N = 2$ in (1.5) we can express the polarization for the signal field as

$$P_s\phi_s = \epsilon_0\chi_s^{(1)}E_s\phi_s + \chi_{sp_s}^{(2b)}E_s^*E_p\phi_s + \chi_{sss}^{(2a)}E_s^2\phi_s^2 + (\chi_{ssp}^{(2a)} + \chi_{sps}^{(2a)})E_sE_p\phi_s^3 + \chi_{spp}^{(2a)}E_p^2\phi_s^4 + \chi_{sss}^{(2b)}E_s^*E_s + \chi_{sps}^{(2b)}E_p^*E_s\phi_s^* + \chi_{spp}^{(2b)}E_p^*E_p.$$

Here the subscripts indicate the fact that the susceptibilities are truly functions of ω and the geometry of the crystal - eg. $\chi_{ssp}^{(2a)} = \chi_{sps}^{(2a)}$ only when the crystal has a particular symmetry. Dividing through by ϕ_s leaves only the first two terms with constant phase, all other terms are highly oscillatory in time and will be neglected in what follows. Retaining only these resonant terms we arrive at the following constitutive equations for the amplitudes of the polarization fields

$$\begin{aligned} P_s &= \epsilon_0\chi^{(1)}E_s + \chi^{2b}E_pE_s^* \\ P_p &= \epsilon_0\chi^{(1)}E_p + \chi^{2a}E_s^2. \end{aligned} \tag{1.6}$$

Formally the susceptibilities are functions of the frequency, $\chi = \chi(\omega)$, but it is reasonable for the frequency range and time-scale of these devices to take them to be constant [5].

Inserting these forms for E_s,E_p, P_s,P_p, k_s and k_p into (1.3) we have

$$\frac{\partial E_s}{\partial t} = \frac{c^2k^2 - \omega^2(1+\chi^1)}{2\omega(1+\chi^1)}E_s + i\frac{c^2}{2\omega(1+\chi^1)}\nabla_r^2E_s + i\frac{\chi^{2b}\omega}{2\epsilon_0(1+\chi^1)}E_pE_s^* - i\frac{\partial^2}{\partial t^2}\left(\frac{1}{2\omega}E_s - \frac{\chi^{2b}}{2\epsilon_0\omega(1+\chi^1)}E_pE_s^*\right) \tag{1.7}$$

$$\frac{\partial E_p}{\partial t} = \frac{c^2k^2 - \omega^2(1+\chi^1)}{4\omega(1+\chi^1)}E_p + i\frac{c^2}{4\omega(1+\chi^1)}\nabla_r^2E_p + i\frac{\chi^{2a}\omega}{2\epsilon_0(1+\chi^1)}E_s^2 - i\frac{\partial^2}{\partial t^2}\left(\frac{1}{2\omega}E_p + \frac{\chi^{2b}}{2\epsilon_0\omega(1+\chi^1)}E_s^2\right)$$

Assuming a perfect cavity to be dispersionless gives rise to the linear dispersion relation

$$k = \frac{\omega}{c}\sqrt{1+\chi^1}, \tag{1.8}$$

derived by setting the coefficients of the first terms on the right hand side of (1.7) to zero. From subsequent analysis it becomes apparent that the second order temporal derivative terms appearing in (1.7) are insignificant at optical frequencies and may be omitted. With this additional simplification and using the dispersion relation (1.8) equation (1.7) reduces to

$$\begin{aligned} \frac{\partial E_s}{\partial t} &= i\frac{c^2}{2\omega(1+\chi^1)}\nabla_r^2E_s + i\frac{\chi^{2b}\omega}{2\epsilon_0(1+\chi^1)}E_pE_s^*, \\ \frac{\partial E_p}{\partial t} &= i\frac{c^2}{4\omega(1+\chi^1)}\nabla_r^2E_p + i\frac{\chi^{2a}\omega}{2\epsilon_0(1+\chi^1)}E_s^2. \end{aligned} \tag{1.9}$$

The derivation of (1.9) has assumed a perfect cavity where no energy is lost out through the mirrors and that the length is an integral number of wave-lengths. A more physically reasonable system is described by adding a linear damping and dispersion term to each of the above equations. The damping comes from leakage out of the cavity over one period and the damping coefficients can be expressed [4]

$$\gamma_s = \frac{cT_s}{L} \qquad \text{and} \qquad \gamma_p = \frac{cT_p}{L}$$

where T_p and T_s are the transmittivities of the mirrors at the indicated frequencies and L is the transverse length of the cavity. Similarly the signal and pump detuning coefficients, δ_s and δ_p, take the form, [4],

$$\delta_s = \omega_1 - \omega \qquad \text{and} \qquad \delta_p = (\omega_2 - 2\omega)\frac{T_s}{T_p}$$

where ω_1 and ω_2 are fundamental modes of the cavity. In the application under consideration the system is being forced at a frequency 2ω with strength P. This leads to the inclusion of a constant P to the driving field equation. With these modifications equation (1.9) takes the form

$$\begin{aligned} \frac{\partial E_s}{\partial t} &= i\frac{c^2}{2\omega(1+\chi^1)}\nabla_r^2 E_s + i\frac{\chi^{2b}\omega}{2\epsilon_0(1+\chi^1)}E_p E_s^* - \gamma_1 E_s - i\delta_s E_s \\ \frac{\partial E_p}{\partial t} &= i\frac{c^2}{4\omega(1+\chi^1)}\nabla_r^2 E_p + i\frac{\chi^{2a}\omega}{2\epsilon_0(1+\chi^1)}E_s^2 - \gamma_2 E_p - i\delta_p E_p + P. \end{aligned} \tag{1.10}$$

Notice now that the dispersion is determined by material properties of the system, not strictly of the incident wave as in (1.7).

To properly scale the equations we introduce the dimensionless quantities

$$\begin{aligned} U &= \frac{\sqrt{ab}}{\gamma_s}E_s, \\ V &= i\frac{\gamma_s}{a}\gamma_p E_p, \\ S &= \frac{\gamma_1^2}{\sqrt{ab}}P, \\ \alpha &= \frac{\gamma_p}{\gamma_s}, \\ \Delta_1 &= \frac{\delta_s}{\gamma_s}, \\ \Delta_2 &= \frac{\delta_p}{\gamma_s}, \\ \tau &= \gamma_s t, \\ \rho &= \frac{\sqrt{2\omega}}{c}r, \end{aligned}$$

where a, b are the coefficients of the nonlinear terms

$$a = \frac{\chi^{2b}\omega}{2\epsilon_0(1+\chi^1)},$$
$$b = \frac{\chi^{2a}\omega}{\epsilon_0(1+\chi^1)}.$$

We arrive at the dimensionless OPO equations

$$\begin{aligned} \frac{\partial U}{\partial \tau} &= i\nabla_\rho^2 U - (1+i\Delta_1)U + U^*V, \\ \frac{\partial V}{\partial \tau} &= \frac{i}{2}\nabla_\rho^2 V - (\alpha+i\Delta_2)V + S - U^2. \end{aligned} \tag{1.11}$$

in which τ is time, ρ is the transverse spatial coordinate, Δ_1 and Δ_2 are the cavity detuning parameters, α is the ratio of the transmittivities of the mirrors in the cavity to the pump and signal frequencies respectively, S is the normalized pump strength and U and V are the normalized complex amplitudes for the signal and pump fields.

These equations may also be derived in a similar physical device with an entirely different geometry - the phase sensitive amplifier [11]. In this context, one is concerned with the amplitude as it changes in the direction of propagation. However, the focus is on a much faster time scale and the so-called optical co-ordinates are used where the Laplacian is with respect to the temporal coordinate (and is thus always in 1 dimension) and the first derivative terms are with respect to the longitudinal spatial variable z.

1.4 Reduction to SPNLS in the large detuning limit

A consequence of using real mirrors and a real nonlinear crystal is that the pump detuning Δ_2 can be moderately large [12]. It may at first seem counterintuitive that the pump detuning would depart significantly from the signal detuning, but the geometry of the cavity is chosen so as to maximize the output of a coherent signal frequency and while the $\omega_p = 2\omega_s$, due to the physical imperfections of the system it is not necessarily true that $\omega_2 \sim 2\omega_1$. Also, the detuning parameters are inversely proportional to the transmittivities of the mirrors at the respective frequencies.

In this thesis, we will consider the so-called focusing case, Δ_1 and $\Delta_2 > 0$. Focusing is a common occurrence in nonlinear optics. In the case of NLS, focusing is distinguished from defocusing by the sign of the non-linearity. Depending upon the space dimension the focusing in NLS can produce (as we shall see) an L^∞ blow-up. Generically, focusing systems concentrate mass whereas defocusing systems equidistribute mass. In one dimension, the canonical solution to a focusing problem is a sech, whereas for defocusing it is a tanh.

In the case of large pump detuning, $\Delta_2 \gg 1$ (1.11) has been reduced [7, 13] to the parametrically forced Nonlinear Schrodinger equation (PNLS). As we shall see, this reduction is adequate in one space dimension but is not a faithful representation in two dimensions. We derive PNLS and a next order correction - saturating PNLS (SPNLS) - which includes higher order dispersive and nonlinear terms, as reductions of the full OPO equations.

From the assumption $\Delta_2 \gg 1$ define

$$\epsilon = \frac{1}{\Delta_2}.$$

In order to compensate for the dispersion in the pump signal, the pump strength must be increased proportionally so that $\frac{S}{\Delta_2} \sim \mathcal{O}(1)$. This leads us to introduce

$$\gamma = \frac{S}{\Delta_2}.$$

Keeping with convention we redefine

$$a = \Delta_1.$$

In order to simplify the full OPO system in the large detuning limit we rescale U

$$U = \frac{1}{\sqrt{\epsilon}}\phi, \tag{1.12}$$

to form a rescaled version of OPO (1.11)

$$\begin{aligned} \phi_t &= i\nabla^2\phi - (1+ia)\phi + i\phi^* V \\ V &= i(\phi^2 - \gamma) + \epsilon\left(iV_t + \frac{1}{2}\nabla^2 V + i\alpha V\right). \end{aligned} \tag{1.13}$$

It is clear from (1.13) that the large detuning limit is a singular perturbation. In such limits, it is often the case that after a rapid initial transient the solution comes to reside on a sub-manifold. Numerical calculations show that V approaches the manifold rapidly for initial conditions $|V_0|_\infty \ll= \frac{1}{\epsilon}$ but that it may not for very large initial data, see figure (1.2a). The form of (1.13) leads us to hope that V is functionally dependent on ϕ and thus make the following assumption on the form of V

$$V = W(\phi), \tag{1.14}$$

where the unknown function W admits an expansion

$$W = W_0 + \epsilon W_1 + \mathcal{O}(\epsilon^2). \tag{1.15}$$

With V given by (1.14) the OPO reduces to a single equation which we call the outer equation

$$\phi_t = i\nabla^2\phi - (1+ia)\phi + i\phi^* W(\phi). \tag{1.16}$$

The first order approximation $W = W_0$ recovers the PNLS equation, while keeping terms to second order, $W = W_0 + \epsilon W_1$, in (1.16) yields the SPNLS equation. The numerical evidence in chapter 2 indicates that the reduction of OPO to SPNLS is qualitatively accurate, even through the dynamics of the saturating blow-up and subsequent radiation and oscillations. We remark here that (1.15) is not a regular perturbation expansion of OPO, such an expansion would include terms for both U and V of the form

$$\begin{aligned} U &= \epsilon^{\alpha_0} U_0 + \epsilon^{\alpha_1} U_1 + \ldots \\ V &= \epsilon^{\beta_0} V_0 + \epsilon^{\beta_1} V_1 + \ldots \end{aligned}$$

This method agrees with ours to first order, (for the derivation of PNLS [7, 13]), but produces a pair of coupled equations for each subsequent order. Such a system is not amenable to the analysis employed here (see chapter 3).

We substitute (1.14) into (1.11) in order to determine W_0 and W_1 as a perturbation series in the order parameter ϵ,

$$\frac{\partial}{\partial t}(W_0 + \epsilon W_1) = \frac{i}{2}\nabla^2 (W_0 + \epsilon W_1) + \frac{\gamma}{\epsilon} - \frac{\phi^2}{\epsilon} - (\alpha + \frac{i}{\epsilon})(W_0 + \epsilon W_1). \tag{1.17}$$

At $\mathcal{O}(1)$ we have the algebraic relation,

$$W_0 = i(\phi^2 - \gamma). \tag{1.18}$$

The equation at $\mathcal{O}(\epsilon)$ is

$$\frac{\partial}{\partial t} W_0 = \frac{i}{2}\nabla^2 W_0 - \alpha W_0 - i W_1,$$

and a substitution for W_0 from (1.18) yields

$$W_1 = -\frac{\partial}{\partial t}\phi^2 + \frac{i}{2}\nabla^2\phi^2 - \alpha(\phi^2 - \gamma). \tag{1.19}$$

At this point we can clearly see the form of all subsequent orders and write down a recursive definition of W

$$W = \sum_{n=0}^{\infty} \epsilon^n W_n$$

where

$$\begin{aligned} W_0 &= i(\phi^2 - \gamma) \\ W_n &= i\frac{\partial W_{n-1}}{\partial t} + \frac{1}{2}\nabla^2 W_{n-1} + i\alpha W_{n-1} \qquad n > 1. \end{aligned} \tag{1.20}$$

This expansion is formal and we may expect convergence only when ϕ and all its derivatives are uniformly bounded. An analysis of the importance of higher order terms at blow-up is given in section 3.5. In figure (1.2a) we see the convergence to the manifold for various initial data V_0 - $V_0 = W_0(\phi), -W_0(\phi), 0$ and purely random data. However, for large initial data $|V_0| \sim \mathcal{O}(\frac{1}{\epsilon})$ the solution does not converge. The convergence of the expansions of W in one dimension are presented in (1.2b).

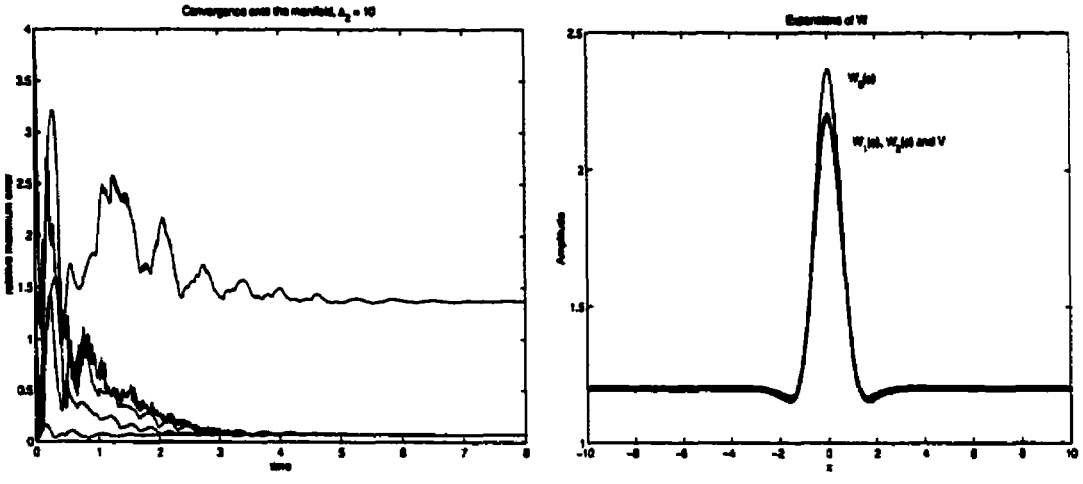

(a) Convergence onto the manifold.

(b) Convergence of W.

Figure 1.2: Agreement with the manifold

From (1.14), (1.18), (1.19) and the equation for U in (1.11) we can find the evolution equation for the rescaled signal field ϕ

$$\phi_t = i\nabla^2\phi - (1+ia)\phi + \phi^* \left(i\phi^2 - \gamma + i\epsilon \left(-\frac{\partial \phi^2}{\partial t} + \frac{i}{2}\nabla^2\phi^2 + \gamma\alpha - \alpha\phi^2 \right) \right) + \mathcal{O}(\epsilon^2).$$

The equalities

$$\frac{\partial \phi^2}{\partial t} = 2\phi\frac{\partial \phi}{\partial t}$$
$$\nabla^2\phi^2 = 2\left(\phi\nabla^2\phi + \left(\frac{\partial \phi}{\partial r} \right)^2 \right).$$

lead us, after dropping $\mathcal{O}(\epsilon^2)$ terms, to a more familiar equation for ϕ; PNLS with higher order corrections,

$$i\phi_t + \nabla^2\phi + |\phi|^2\phi + (i-a)\phi - \gamma\phi^* =$$
$$i\epsilon\left(-2|\phi|^2\phi_t + i|\phi|^2\nabla^2\phi + i(\phi_r)^2\phi^* - \gamma\alpha\phi^* + \alpha|\phi|^2\phi \right) \quad (1.21)$$

All the terms on the right-hand side of (1.21) are small except when ϕ is near blow-up in which case the quantities $|(\phi_r)^2|, |\phi_t|$ and $|\nabla^2\phi|$ dominate $|\phi|$. Re-writing (1.21) by gathering like terms we have SPNLS

$$i\phi_t(1+2\epsilon|\phi|^2)+\nabla^2\phi(1+\epsilon|\phi|^2)+|\phi|^2\phi+(i-a)\phi-\gamma\phi^*+\epsilon(\phi_r)^2\phi^*=0. \tag{1.22}$$

A different formulation is obtained by dividing (1.22) through by $(1+2\epsilon|\phi|^2)$

$$i\phi_t+\nabla^2\phi\frac{1+\epsilon|\phi|^2}{1+2\epsilon|\phi|^2}+\frac{|\phi|^2\phi}{1+2\epsilon|\phi|^2}+(i-a)\frac{\phi}{1+2\epsilon|\phi|^2}-\gamma\frac{\phi^*}{1+2\epsilon|\phi|^2}+\epsilon\frac{(\phi_r)^2\phi^*}{1+2\epsilon|\phi|^2}=0 \tag{1.23}$$

which is suggestive of the saturating NLS (SNLS)

$$i\phi_t+\nabla^2\phi+\frac{|\phi|^2\phi}{1+\epsilon|\phi|^2}=0 \qquad \epsilon\ll 1. \tag{1.24}$$

The SNLS equation has been derived as a regularization of NLS in many physical contexts - see [17] and the references therein.

We also note that the case $\epsilon=0$ in (1.22) permits us to recover the parametrically forced nonlinear Schrodinger equation

$$i\phi_t+\nabla^2\phi+|\phi|^2\phi+(i-a)\phi-\gamma\phi^*=0. \tag{1.25}$$

which has been derived not only as a model for the optical parametric oscillator but also for Faraday resonance in water, parametric instabilities for plasma waves, the parametric generation of spin waves and also magnetic solitons in ferro-magnets and anti-ferro-magnets (see [14] and the references therein). PNLS has been studied analytically in [13, 14, 15]. Although much of the analysis for PNLS is similar to that of NLS, it is not identical as the addition of the conjugate term means that PNLS is not a Hamiltonian system.

Chapter 2

Numerical comparison of OPO, PNLS and SPNLS

Although the OPO equations are naturally posed in two spatial dimensions, it is reasonable to discuss the equations in one space dimension assuming uniformity in the transverse direction or when considering the phase sensitive amplifier. In the defocusing case OPO and PNLS have been shown to be in good agreement [5]. The stability of pulses and fronts for the focusing and defocusing PNLS respectively has been established [13] for a wide range of parameters for which the PNLS is a good reduction of the full OPO. We compare pulse solutions to OPO to exact solutions of PNLS, and compare stability properties of both systems.

For a discussion of the numerical methods used, please refer to chapter 4.

2.1 Exact PNLS solutions in 1D

Because NLS is well-posed in one spatial dimension, one would expect solutions of SPNLS, PNLS and, hopefully, OPO to be well-behaved as well. Indeed, in this setting, SPNLS exhibits only small quantitative differences from PNLS and so we restrict our attention to PNLS in one space dimension

$$i\frac{\partial\phi}{\partial t}+\frac{\partial^2\phi}{\partial x^2}+|\phi|^2\phi+(i-\alpha)\phi-\gamma\phi^*=0 \tag{2.1}$$

as a reduction to (1.22).

Exact stationary pulse-like solutions to PNLS can by constructed from the form $\phi = f(x)e^{i\theta}$ where the real-valued function $f(x)$ and constant θ are to be determined. Inserting this ansatz into

(2.1) we obtain the equation

$$\frac{d^2f}{dx^2} + f^3 + (i-a)f - \gamma f e^{-2i\theta} = 0. \tag{2.2}$$

For both a and γ real, we separate (2.2) into its real and imaginary parts producing two equations

$$\frac{d^2f}{dx^2} + f^3 - (a + \gamma\cos 2\theta)f = 0, \tag{2.3}$$

$$f(1 + \gamma\sin 2\theta) = 0. \tag{2.4}$$

The relation (2.4) implies that $\theta = -\frac{1}{2}\sin^{-1}\frac{1}{\gamma}$ which requires $\gamma \geq 1$. This inequality comes as no surprise; it indicates a critical pumping strength necessary to overcome the damping. Indeed for $\gamma < 1$, it is easy to see that any solution to the initial value problem associated to (2.1) decays exponentially to zero. With θ prescribed as above the equation for f reduces to

$$\frac{d^2f}{dx^2} + f^3 - \alpha_\pm f = 0, \tag{2.5}$$

where $\alpha_\pm = a \pm \sqrt{\gamma^2 - 1}$. The two values $\alpha_\pm$ arise from the two branches of $\sin^{-1}$. Equation (2.5) is easily solved under the conditions that $\lim_{x\to\infty} f(x) = 0$, $\lim_{x\to\infty} \frac{df}{dx} = 0$ and $\alpha_\pm \geq 0$

$$f_\pm = \sqrt{2\alpha_\pm}\,\mathrm{sech}\sqrt{\alpha_\pm}x,$$

thus the solutions to (2.1) are

$$\phi_\pm = e^{i\theta_\pm}\sqrt{2(a \pm \sqrt{\gamma^2-1})}\,\mathrm{sech}(\sqrt{a \pm \sqrt{\gamma^2-1}}x), \tag{2.6}$$

where $\theta_\pm = -\frac{1}{2}\sin^{-1}\frac{1}{\gamma}$ correspond to $\alpha_\pm$ respectively with $\theta_+ \in \left(-\frac{\pi}{2}, \frac{\pi}{2}\right]$ and $\theta_- = \theta_+ + \pi$.

2.2 Numerical comparison of transverse OPO to 1D PNLS

By extension onto the manifold $\mathcal{W}$, stationary solutions of PNLS yield approximate stationary solutions of the rescaled OPO,

$$\begin{aligned} U &= \frac{\phi}{\sqrt{\epsilon}} \\ V &= \mathcal{W}_0(\phi) \\ &= i(\phi^2 - \gamma). \end{aligned}$$

The so-called down solution, ϕ_-, can be shown to be unstable to perturbations [14]. The OPO shares this property, that is solutions integrated from initial data $U = \frac{\phi_-}{\sqrt{\epsilon}}$, $V = i(\phi_-^2 - \gamma)$ decay to zero exponentially fast. The agreement between OPO for initial conditions of the form $U = \frac{\phi_+}{\sqrt{\epsilon}}$, $V =$

$i(\phi_+^2 - \gamma)$, and PNLS is quite good over a wide set of parameters. The amplitude of the up solution, ϕ_+, to PNLS with parameter values a, γ is seen from (2.6) to be given by by $\sqrt{2a + 2\sqrt{\gamma^2 - 1}}$. Quite good agreement to this is achieved by OPO as well, as seen in figure (2.1a). The exact solutions of PNLS, ϕ_-, with amplitudes $\sqrt{2a - 2\sqrt{\gamma^2 - 1}}$, are unstable and as OPO shares that instability no nearby solutions are obtainable. The known stability of ϕ_+ [13] in the (a, γ) plane is indicated by

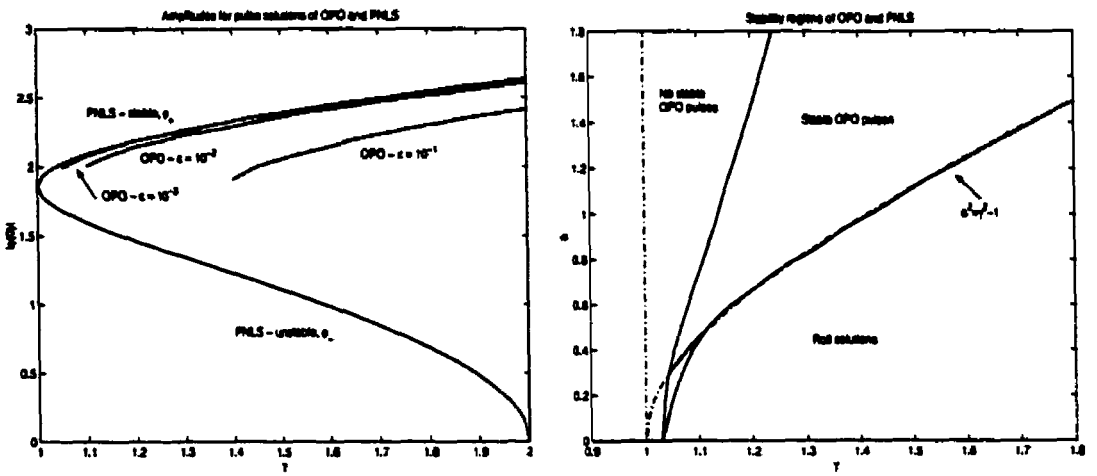

(a) Bifurcation in the amplitude of ϕ with $a = \sqrt{3}$.

(b) Stability of PNLS and OPO.

Figure 2.1: Agreement with the manifold

the dashed lines in figure (2.1b). For $\gamma < 1$ ϕ_+ is unstable, for $1 < \gamma < \sqrt{1 + a^2}$ it is stable and for $\gamma > \sqrt{1 + a^2}$, ϕ_+ is unstable and leads to roll solutions. To compare the stability properties of OPO to PNLS we have numerically integrated OPO with various values of S and Δ_1 at fixed Δ_2 with initial conditions

$$\begin{aligned} U_0 &= \frac{\phi_+^2(1+g)}{\sqrt{\epsilon}} \\ V_0 &= i(\phi_+^2 - \gamma) \end{aligned}$$

where g is a small ($\max|g| < .01$) random perturbation. The results of these computations are summarized in figure (2.1b) where we see there is excellent qualitative agreement.

It is not only the amplitudes that agree well in the stable region, but the full profile. There is an essential bifurcation for $\gamma = \sqrt{a^2 + 1}$, in the over-pumped region, $\gamma > \sqrt{1 + a^2}$, the most interesting behaviour is obtained and the first qualitative differences between OPO and PNLS can be seen. Taking as initial data a perturbed pulse for both OPO and PNLS, we can compare the two systems as they evolve in time. We see that about the fixed central pulse two new pulses grow out on either

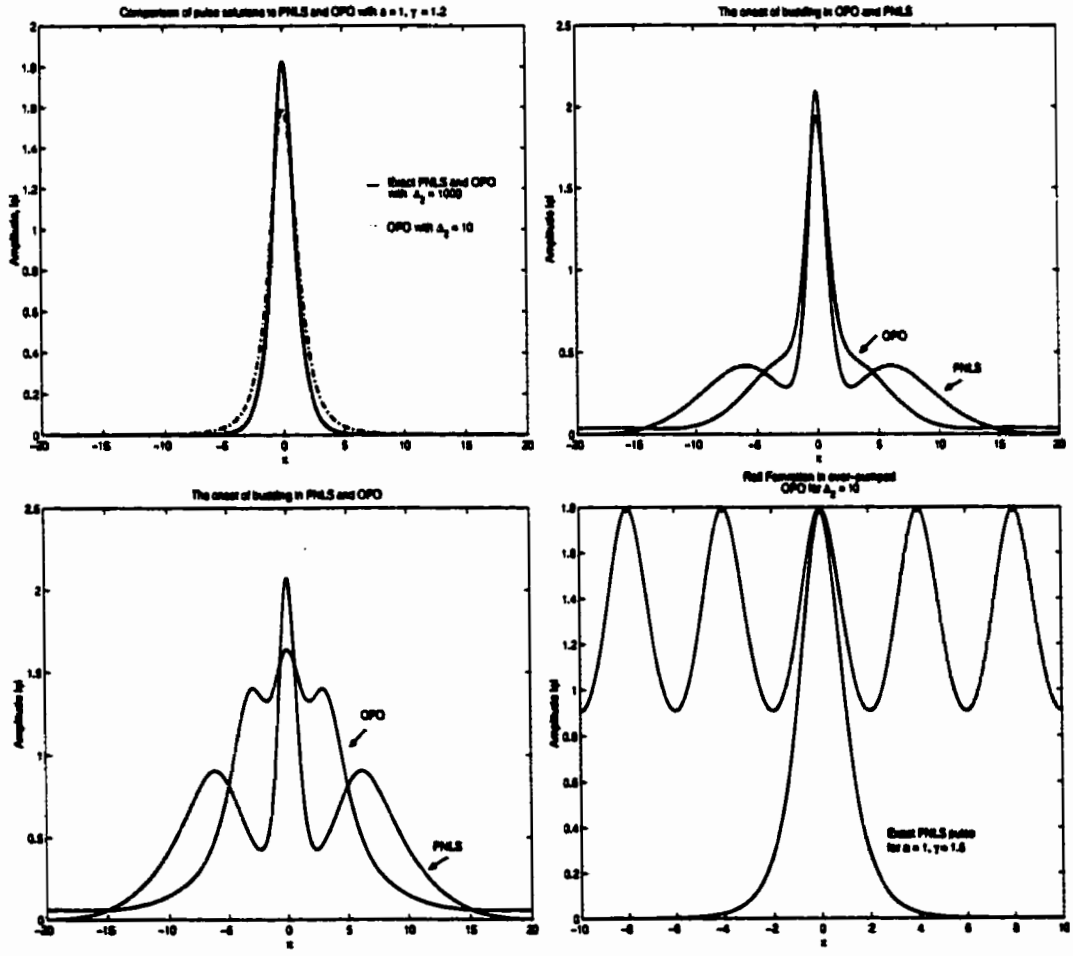

Figure 2.2: Comparison of profiles of solutions to PNLS and OPO

side in a process we have (mis-)named Budding. The buds on OPO grow out from the tip of the pulse akin to pulse splitting, while those for PNLS arise from the base of the central pulse and grow. The comparison of pulse profiles and roll solutions for PNLS and OPO is described in figure (2.2). Most interesting is the fact that the OPO pulse does not bud locally but rather distributes some mass all along the line first. In particular it takes longer for OPO to bud on a larger domain, which is not the case for PNLS. In practice this might mean that OPO would not bud as the boundary effects could become very important.

The long term behaviour for both systems is qualitatively the same - each develops a chain of N pulses with the amplitude for PNLS given exactly by $\sqrt{2\alpha_+}$ and approximately so for OPO. Although OPO can appear stable, the pulses jostle endlessly, but on a much slower time scale than PNLS. These periodic solutions are really roll solutions as have been observed in the 2 dimensional case in a different parameter regime. Close to the essential bifurcation one can reduce OPO to a modified Swift-Hohenberg equation [4] so the rolls are perhaps expected. Once the roll state has been reached, PNLS again captures the features of OPO very well. The rolls for both OPO and PNLS have very similar amplitudes and periods. However, it is not clear that OPO would reach a roll state for other than periodic boundary conditions, whereas PNLS seems quite happy to.

2.3 Numerical comparison of OPO to 2D PNLS and SPNLS

While in one space dimension PNLS is a reasonable reduction of OPO, in two dimensions, this is not always the case. Figure (2.3) shows that PNLS exhibits blow-up for many initial conditions and parameter values.

In contrast, we see in figure (2.4) that both OPO and SPNLS saturate even for the small value of $\epsilon = 10^{-6}$. Notice that for this value of ϵ both and OPO and SPNLS closely follow PNLS well into the blow-up stage.

Motivated by the numerical evidence of blow-up in the PNLS and that in the limit of large Δ_2, OPO follows PNLS for some time, we consider the blow-up in PNLS more carefully.

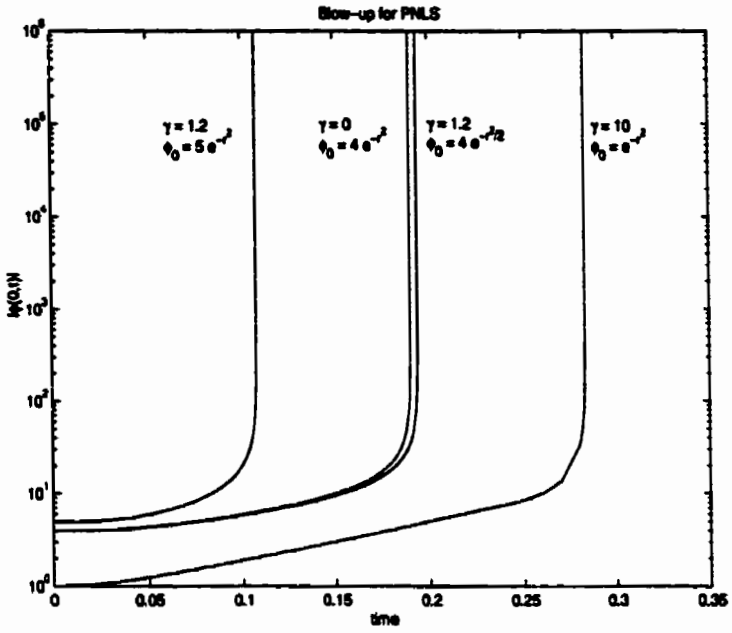

Figure 2.3: Blow-up in PNLS for various parameters and initial data.

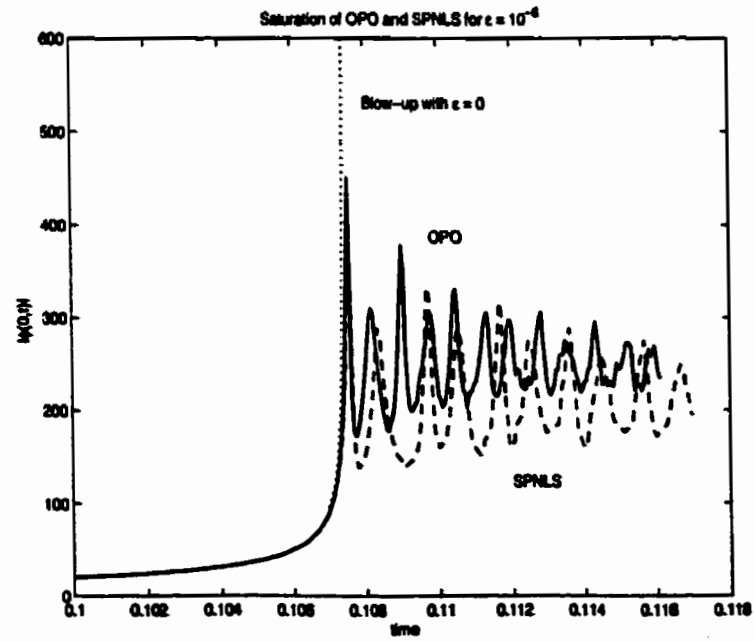

Figure 2.4: Saturation of OPO and PNLS

2.4 Numerical analysis of blow-up in 2D PNLS

It is well known that solutions to NLS in more than 2 dimensions are self-similar and that they are approximately self-similar in 2 dimensions [17]. Self-similar means that there exist functions f and g and a profile P such that the function ϕ satisfying

$$\phi(r,t) = \frac{1}{f(t)} P\left(\frac{r}{g(t)}\right)$$

solves NLS and moreover with $lim_{t\to t^*} f = 0$ and $lim_{t\to t^*} g = 0$. One observes the same form with a small correction for approximately self-similar solutions

$$\phi(r,t) = \frac{1}{f(t)} P\left(\frac{r}{g(t)}\right) + \mathcal{O}(f(t))$$

Thus for self-similar problems we can concentrate on finding the blow-up rate, $f(t)$, the spatial rescaling $g(t)$ and the profile $P(\rho)$. It is well known for NLS that the spatial profile is determined by the Townes soliton (section 3.2) which we denote $R(\rho)$. Ignoring the details of the profile for the moment, we can see that the solutions to PNLS do in fact approach the Townes near blow-up. Taking the Townes as the spatial profile in the asymptotic limit, in figure (2.5) we plot $\frac{\phi}{L}$ over $0 \leq \rho \leq 8$ with $L = \frac{|\phi(0,t)|}{R(0)}$, $\rho = \frac{r}{L}$ for various times approaching the blow-up - $10^{-2} \leq L < 10^{-6}$. We can also clearly see that the blow-up rate is given by $f = A\sqrt{\frac{\log|\log t^* - t|}{t^* - t}}$. Plotting $f_i(t)|\phi(0,t)|$ with

$$f_1 = \frac{A}{\sqrt{t^* - t}} \qquad \text{and} \qquad f_2 = A\sqrt{\frac{\log|\log t^* - t|}{t^* - t}}$$

against a scaled time $\tau = \log\frac{t^*}{t^* - t}$ we see that $\frac{|\phi(0,t)|}{\sqrt{t^* - t}}$ grows whereas $\sqrt{\frac{\log|\log t^* - t|}{t^* - t}}|\phi(0,t)|$ approaches a constant. In this plot $|\phi|$ ranges from 20 to 350000. For comparison we also include rescaled solutions to OPO and SPNLS with $\epsilon = 10^{-6}$. Here the central pulse regions agree well, but not the distant behaviour.

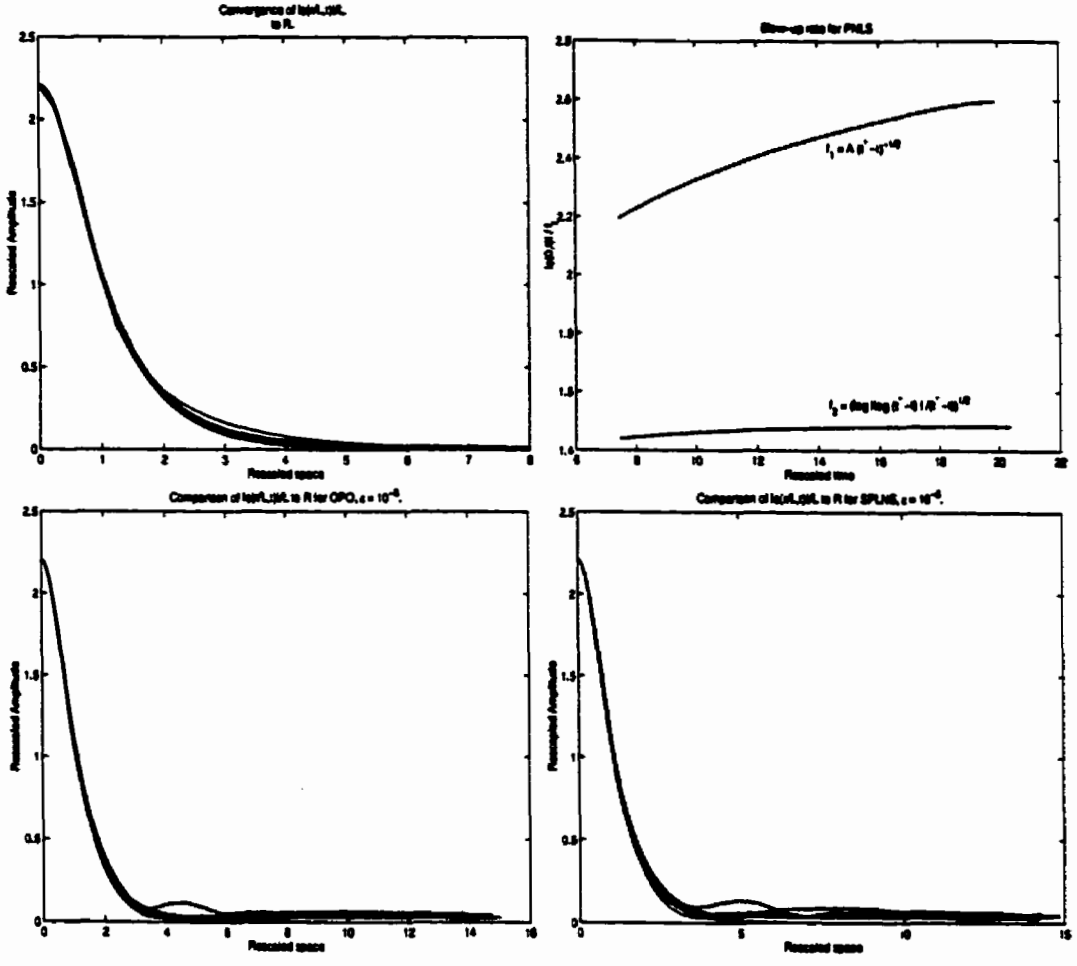

Figure 2.5: Convergence of PNLS to self-similar solutions.

While the rate and profile for blow-up are the same for NLS and PNLS, initial conditions that lead to blow-up in one do not necessarily lead to blow-up in the other. For instance, for a value of $\gamma = 1.2$, and the commonly used initial conditions, $\phi_0 = 4e^{-r^2}$ PNLS does not blow-up while NLS does. This effect is perhaps related to what is observed in stochastic NLS [16]

$$i\phi_t + \nabla^2\phi + |\phi|^2\phi + \delta(t)\phi = 0,$$

with δ being a small random parameter, where blow-up can be arrested for moderate values of $\langle\delta^2\rangle$. As seen in figure (2.6) for large pumping, some small initial data can lead to blow-up in PNLS whereas the corresponding solutions of NLS do not.

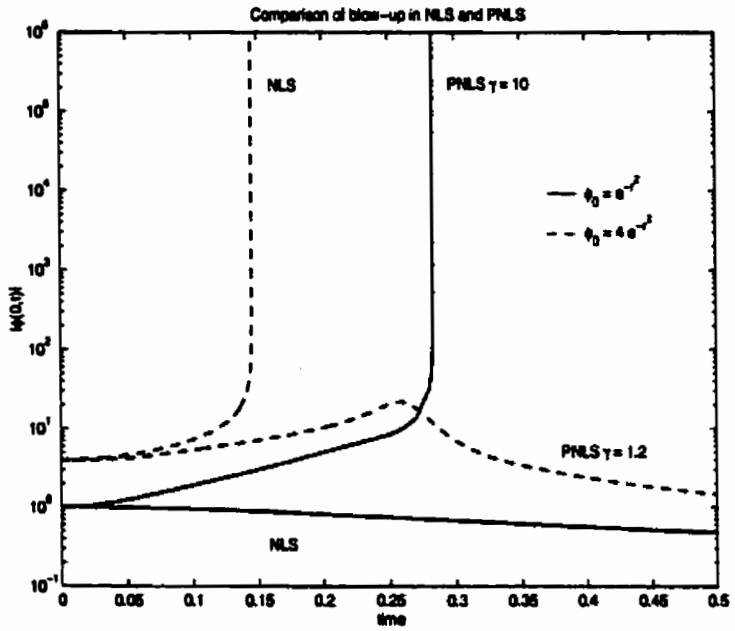

Figure 2.6: Comparison of blow-up of NLS and PNLS with different initial data.

Chapter 3

Analysis of the saturating blow-up

3.1 Review of focusing NLS in 2 dimensions

Numerical simulation in two-dimensions of elliptical and non-symmetric initial data suggest that blow-up is a radial phenomenon, hence while working in two spatial dimensions we will consider only radially symmetric solutions. For NLS the case of two dimensions is critical because for $d < 2$ there is no blow-up and for $d > 2$ there is self-similar blow-up. Both numerical and rigorous analysis are notoriously difficult in two dimensions.

We can study the blow-up in PNLS in much the same manner as in NLS due to their similarities (section 2.4). There is much numerical and analytical evidence (see [17] and the references therein and [26]) that the NLS equation

$$\begin{aligned} i\phi_t + \nabla^2\phi + |\phi|^2\phi &= 0 \\ \phi(r,t) &= \phi_0(r) \end{aligned} \tag{3.1}$$

possess approximately self-similar finite-time blow-up solutions in two space dimensions. Finite-time blow-up in the context of NLS means there exists $t^* < \infty$ such that a solution ϕ exists for $0 < t < t^*$ but that $\lim_{t\to t^*} \|\phi(r,t)\|_\infty = \infty$. It is easily demonstrated that strong solutions must break down in finite time. The NLS equation has infinitely many conserved quantities, one of which, the Hamiltonian, is defined in radial variables as

$$H(t) = \int_0^\infty \left(|\phi_r|^2 - \frac{1}{2}|\phi|^2 \right) r\, dr. \tag{3.2}$$

If we also define the variance as

$$V(t) = \int |\phi|^2 r^3\, dr, \tag{3.3}$$

then a simple calculation shows that

$$\frac{d^2V}{dt^2} = 8\,H(t), \tag{3.4}$$

but for a classical solution $\frac{dH}{dt} = 0$, and we can integrate (3.4) immediately to obtain

$$V(t) = 4\,H\,t^2 + V'(0)\,t + V(0). \tag{3.5}$$

From its definition $V(t) > 0$; but if $H = H(\phi_0) < 0$ then we reach a contradiction. Indeed for $H(\phi_0) < 0$ (3.5) implies that there exists a time t^* such that $V(t^*) = 0$ which contradicts (3.3). Thus the solution must lose regularity before $t = t^*$. This is seen from numerical calculations as $\lim_{t\to t^*} \|\phi(t,\cdot)\|_\infty = \infty$ despite conservation of mass which implies $\lim_{t\to t^*} \|\phi(t,\cdot)\|_2 = \|\phi_0\|_2$!

3.1.1 The Townes Soliton

Much of the analysis of NLS involves a special solution called the Townes soliton which is the spatial component of a separable solution of the form $\phi = e^{it}R(r)$. The Townes soliton, R, is defined as the positive, monotonically decreasing solution to

$$\begin{aligned} &\nabla^2 R + R^3 - R = 0 \\ &R'(0) = 0 \\ &\lim_{r\to\infty} R = 0. \end{aligned} \tag{3.6}$$

It can been shown, [18], that (3.6) has a unique solution given the constraints on positivity and monotonicity. The Townes is important in the study of NLS because numerically it is seen ([17] and section 2.4) that near blow-up solutions are roughly rescaled Townes solitons, $\phi \sim \frac{1}{L}R(\frac{r}{L})$. As we have already seen, this is true for PNLS as well. This is expected since the terms by which PNLS and NLS differ are linear and are asymptotically weak blow-up where the nonlinearity and derivative terms dominate.

For the Townes soliton we have two important facts: the Hamiltonian $H(R) \equiv 0$ and for any initial data ϕ_0 the corresponding solution may blow-up in finite time only if $\int_0^\infty |\phi_0|^2 r\,dr \geq N_c$ where we have defined $N_c \equiv \int_0^\infty R^2 r\,dr$. Also, using the Townes soliton one can construct an exact, self-similar blow-up solution of the form

$$\phi(r,t) = \frac{1}{\sqrt{t^*-t}} e^{\frac{r^2}{4i(t^*-t)}} R\left(\frac{r}{t^*-t}\right).$$

This solution is unstable and is not seen numerically. Numerical evidence, [17], shows the splitting of the pulse into two distinct pieces, $\phi = \phi_s + \phi_{rad}$ where ϕ_s is the modulated Townes soliton and ϕ_{rad} consists of small amplitude dispersing radiation.

Additionally it is known, [18], that R takes the form $R \to \frac{A_r}{e^r\sqrt{r}}$ with $A_r \sim 3.52$, asymptotically as $r \to \infty$.

3.2 Modulational approach to perturbed NLS equations

Following the analysis for blow-up in perturbed NLS equations by Papanicolau and Fibich [19], we can construct an ordinary differential equation for the modulation parameter, $L(t)$.

The overwhelming evidence is that near blow-up solutions to NLS have asymptotic form

$$\phi = \begin{cases} \phi_s, & \text{if } r < \rho_c L(t); \\ \phi_{\text{rad}}, & \text{else.} \end{cases}$$

$$\phi_s \sim \frac{1}{L} V(\zeta, \rho)\, e^{iS},$$

where $\lim_{t\to t^*} V = R$, $\lim_{t\to t^*} L = 0$ and ρ_c is a constant. For the solution to the SPNLS equation we take the form above with $S = \zeta + f(\rho, L, L_t)$, resulting in the ansatz

$$\phi_s(r,t) = \frac{1}{L(t)} V(\zeta,\rho)\, e^{i\zeta + if(\rho,L,L_t)}, \tag{3.7}$$

with $\rho = \frac{r}{L(t)^\alpha}$ and α, ζ and f to be determined. Inserting the ansatz in SPNLS we have

$$i\left(-\frac{L_t}{L^2}V + \frac{1}{L}V_\zeta \zeta_t + \frac{1}{L}V_\rho \rho_t + i\frac{V}{L}(\zeta_t + f_t)\right)e^{iS} + \frac{1}{L^{1+2\alpha}}\nabla_\rho^2\left(Ve^{iS}\right) + \frac{1}{L^3}|V|^2 V e^{iS}$$
$$+ (i-a)\frac{V}{L}e^{iS} - \gamma\frac{V^*}{L}e^{-iS} + \epsilon F\left(\frac{V}{L}e^{iS}\right) = 0, \tag{3.8}$$

where

$$F = i2|\phi|^2\phi_t + |\phi|^2\nabla^2\phi +, (\phi_r)^2\phi^* \tag{3.9}$$

represents the perturbation terms present in (1.22).

To balance the nonlinearity and derivative terms we choose $\alpha = 1$ and $\zeta_t = \frac{1}{L^2}$. With these scalings we return to (3.8) to determine f

$$\frac{1}{L^3}\left(iV_\zeta + |V|^2V + \nabla_\rho^2 V - V\right)e^{iS} + \frac{1}{L}(i-a)Ve^{iS} - \frac{\gamma}{L}V^*e^{-iS}$$
$$+ \left(-i\frac{L_t}{L^2} - \frac{f_t}{L} + i\frac{1}{L^2}\nabla_\rho^2 f - \frac{f_\rho^2}{L^2}\right)Ve^{iS} + \left(-i\frac{L_t}{L}\rho + 2if_\rho\right)V_\rho e^{iS} = 0.$$

Demanding that the coefficient of the V_ρ term be zero, we find that $f = \frac{\rho^2}{4}L_t L$. The coefficient of the V term becomes $\frac{\beta}{4}\rho^2$ with $\beta = -L_{tt}L^3$.

Putting the completed ansatz into SPNLS and changing variables, we get a PDE for V

$$iV_\zeta + \nabla^2 V - V + |V|^2 V + \frac{1}{4}\beta\rho^2 V + L^2((i-a)V - \gamma V^* e^{-2iS}) + L^3 \epsilon F\left(\frac{V(\zeta,\rho)}{L(t)} e^{iS}\right) e^{-iS} = 0 \quad (3.10)$$

where

$$S = \zeta + \frac{L_t L \rho^2}{4}, \quad (3.11)$$

$$\zeta_t = \frac{1}{L^2}, \quad (3.12)$$

$$\beta = -L_{tt} L^3. \quad (3.13)$$

We assume that β, ϵF and L^2 are small, and that to leading order V is the Townes soliton. We write $V = R + u + iv + o(\epsilon, \beta, L^2)$ for u and v real, and separate (3.10) into real and imaginary parts. Under a quasi-steady state assumption (see Fibich and Papanicolau [19]) on u and v and find at second order

$$\mathcal{L}_+ u = -\beta\frac{1}{4}\rho^2 R + L^2(a + \gamma\cos 2S)R - \epsilon L^3 \Re\left(F\left(\frac{R}{L(t)}e^{iS}\right)e^{-iS}\right), \quad (3.14)$$

$$\mathcal{L}_- v = -L^2(1 + \gamma\sin 2S)R - (u)_\zeta - \epsilon L^3 \Im\left(F\left(\frac{R}{L(t)}e^{iS}\right)e^{-iS}\right), \quad (3.15)$$

where the operators $\mathcal{L}_+$ and $\mathcal{L}_-$ are given by

$$\mathcal{L}_+ = \nabla^2 + 3R^2 - 1 \quad \text{and} \quad \mathcal{L}_- = \nabla^2 + R^2 - 1. \quad (3.16)$$

Because we are looking for radial solutions which decay at infinity, we impose the boundary conditions

$$\frac{\partial u}{\partial \rho}(\zeta, \rho = 0) = 0,$$

$$\lim_{\rho\to\infty} u = 0,$$

$$\frac{\partial v}{\partial \rho}(\zeta, \rho = 0) = 0,$$

$$\lim_{\rho\to\infty} v = 0.$$

Due to the quasi-steady state assumption, ζ appears only as a parameter in the forcing terms. We assume u has the form

$$u \sim \beta g(\rho) + \epsilon h(\zeta, \rho) + L^2 l(\zeta, \rho) + o(\beta, \epsilon, L^2). \quad (3.17)$$

Inserting this form for u into (3.14) and equating coefficients of ϵ, β and L^2 gives the following

equations for g, h and l

$$\mathcal{L}_+ g = -\frac{1}{4}\rho^2 R, \qquad g'(0) = 0, \qquad \lim_{\rho\to\infty} g = 0 \tag{3.18}$$

$$\mathcal{L}_+ h = -L^3 \Re\left(F\left(\frac{R}{L}e^{iS}\right)e^{-iS}\right), \qquad \frac{\partial h}{\partial \rho}(\zeta, \rho = 0) = 0, \quad \lim_{\rho\to\infty} h = 0 \tag{3.19}$$

$$\mathcal{L}_+ l = (a + \gamma\cos 2S)R, \qquad \frac{\partial l}{\partial \rho}(\zeta, \rho = 0) = 0, \quad \lim_{\rho\to\infty} l = 0. \tag{3.20}$$

Note that for h and l, ζ is a parameter which affects only the right hand sides. Although not solvable explicitly, each of these equations can be solved - as will be seen shortly.

3.2.1 Solvability conditions

To be able to solve (3.15), we need a solvability condition. Working in a radial space

$$L^2_r(\mathbb{R}_+;\mathbb{R}) = \{f : (0,\infty) \to (-\infty,\infty) \mid \|f\|_2 < \infty, f'(0) = 0\}$$

with the norm

$$\|f\|_2^2 = \int_0^\infty f^2 r dr$$

then the operators $\mathcal{L}_+$ and $\mathcal{L}_-$ are self-adjoint with respect to the inner product

$$(f,g) = \int_0^\infty fgr dr$$

and the following lemmas hold.

Lemma 1 *Given*

$$\mathcal{L}_- f = \nabla^2 f + R^2 f - f = q(r) \tag{3.21}$$

where R is the Townes soliton and q is a real-valued radial function then a solution for f exists if and only if

$$\int_0^\infty Rqr dr = 0.$$

PROOF. To determine the solvability condition for f, we need to determine the nullspace of the operator $\mathcal{L}_-$. Recall that $\mathcal{L}_- R = 0$. To look for additional components of the kernel we use variation of parameters. Assume that $v = uR$ and that $\mathcal{L}_- v = 0$, then

$$2u_r R_r + Ru_{rr} + \frac{1}{r}Ru_r = 0.$$

Solving this directly yields $v = R\int \frac{1}{sR^2}ds$. But, recalling the asymptotic behaviour of R, $R \sim \frac{Ae^{-r}}{\sqrt{r}e^r}$ we see that $v \notin L^2_r(\mathbb{R}_+;\mathbb{R})$ and thus not in the kernel. As $\mathcal{N}(\mathcal{L}_-) = \text{span}\{R\}$, the Fredholm alternative requires that $\int_0^\infty q\,Rrdr = 0$ to solve (3.21). ★

To be certain that we can solve (3.18) - (3.20) we also must consider $\mathcal{L}_+$. Despite the claim of Fibich and Papanicolau to the contrary, [19],

$$\frac{\partial}{\partial r}\mathcal{L}_-R = 0 \Rightarrow \mathcal{L}_+R_r = \frac{R_r}{r^2},$$

that is, R_r is not in the kernel of $\mathcal{L}_+$. To better understand the kernel of $\mathcal{L}_+$ it is best to consider the full two-dimensional problem and then look for solutions with radial symmetry. First we need to construct some eigenfunctions of

$$\mathcal{L}_+^{(2)} = \frac{\partial^2}{\partial r^2} + \frac{1}{r}\frac{\partial}{\partial r} + \frac{1}{r^2}\frac{\partial^2}{\partial\theta^2} + 3R^2 - 1. \tag{3.22}$$

From the calculation above we see immediately that

$$\mathcal{L}_+^{(2)}(\sin(\theta)R_r) = \mathcal{L}_+^{(2)}(\cos(\theta)R_r) = 0$$

where of course $R_r\sin(\theta) = R_y$ and $R_r\cos(\theta) = R_x$ are the translational symmetries of the Townes in two dimensions. A calculation substantively identical to that presented in Lemma 1 shows that there are no additional separable solutions in $\mathcal{N}\left(\mathcal{L}_+^{(2)}\right)$. Eigenfunctions arise with symmetries in equations - with R_x corresponding to translational invariance - thus it is natural in two dimensions to find R_x and R_y rather than R_r in the kernel; only in one space dimension is $R_x = R_r \in \mathcal{N}(\mathcal{L}_+)$.

Lemma 2 *Given*

$$\mathcal{L}_+f = \nabla^2 f + 3R^2 f - f = p(r)$$

where R is the Townes soliton and p is a real-valued radial function then a solution for f exists for all functions $p(r)$ in the space $L^2_r(\mathbb{R}_+;\mathbb{R})$, that is there is no function $v \in L^2_r(\mathbb{R}_+;\mathbb{R})$ such that $\mathcal{L}_+v = 0$.

PROOF. An eigenfunction of $\mathcal{L}_+$ in $L^2_r(\mathbb{R}_+;\mathbb{R})$ solves

$$\begin{aligned} &\nabla^2 v + (3R^2 - 1)v = 0 \\ &v'(0) = 0. \end{aligned} \tag{3.23}$$

Although not solvable exactly, because $R \to 0$ exponentially as $r \to \infty$, we may reduce (3.23) to a solvable problem asymptotically as $r \to \infty$,

$$\nabla^2 v - v = 0. \tag{3.24}$$

By comparison of solutions of (3.23) to those of (3.24) we have, by Sturm's comparison theorem, [21], that a solution to (3.23) can have at most one zero for $r \in (0, \infty)$. A simple calculation,

$$\begin{aligned}(2R^2, v) &= (\mathcal{L}_+ R, v) \\ &= (R, \mathcal{L}_+ v) \\ &= 0 \qquad \text{for } v, \text{ a solution to (3.23)},\end{aligned}$$

shows that v is either identically zero or not sign definite and thus has at least one zero. Hence, if a non-trivial function v solves (3.23), then v has exactly one zero. Without loss of generality we take $v(0) = 1$; any solution bounded at the origin is then of the form αv for some constant α. A solution which is unbounded at the origin is clearly not in $L^2_r(\mathbb{R}_+; \mathbb{R})$ and needs no further attention. To show that there is no solution to (3.23) with $v(0) = 1$ we we consider a hybrid numerical proof. Defining polar co-ordinates

$$v(r) = \rho(r)\cos(\theta(r)) \quad \text{and} \quad v'(r) = \rho(r)\sin(\theta(r)),$$

from (3.23) we have a differential equation for $\theta(r)$

$$\frac{d\theta}{dr} = f(\theta, r) = (1 - 3R^2)\cos^2(\theta) - \frac{\cos(\theta)\sin(\theta)}{r} - \sin^2(\theta), \tag{3.25}$$

from which we have

1. when $v = 0$, $\theta \equiv \frac{\pi}{2}(\mod \pi)$, and $\frac{d\theta}{dr} < 0$,
2. when $v' = 0$, $\theta \equiv 0(\mod \pi)$, and $\frac{d\theta}{dr}$ has the same sign as $1 - 3R^2$.

Additionally (3.23) gives a differential equation for $\rho(r)$

$$\frac{d\rho}{dr} = \rho\left(\sin(\theta)\cos(\theta)(2 - 3R^2) - \frac{\sin^2(\theta)}{r}\right). \tag{3.26}$$

Hence the third quadrant is positively invariant under (3.25) whenever $1 - 3R^2 > 0$; thus if $3R^2 - 1 < 0$, $v < 0$ and $v' < 0$ simultaneously then $vv' > 0$ and v^2 is strictly increasing. Defining r_1 such that $v(r_1) = 0$, r_2 such that $3R^2(r_2) - 1 = 0$ and $r^* = \max(r_1, r_2)$ then we need only integrate (3.23) numerically to $r = r^*$ and check all the negativity conditions. Performing such an integration shows that the conditions are met, thus $\lim_{r\to\infty} v(r) = -\infty$ and $v \notin L^2_r(\mathbb{R}_+; \mathbb{R})$. ★

Additionally, from (3.25) we see that in the limit $r \to \infty$, the steady state solutions are $\theta = \frac{5\pi}{4}$ and $\frac{3\pi}{4}$, with $\theta = \frac{5\pi}{4}$ being stable and $\theta = \frac{3\pi}{4}$ unstable. (We need only consider limiting values of $\theta \in (\frac{\pi}{2}, \frac{3\pi}{2})$ as $\theta(0) = 0$ and we have shown v has exactly one zero.) Equation (3.26) shows that for $r \gg 1$, $\rho' \sim \rho\sin(2\theta)$, thus when $\theta \sim \frac{5\pi}{4}$, $\rho' \sim \rho$ and v has exponential growth, but when $\theta \sim \frac{3\pi}{4}$,

$\rho' \sim -\rho$ and v decays exponentially. For $r < r_{crit} \sim 1.4575$ the third quadrant is not trapping and it is possible for solutions to enter the fourth quadrant. In figure (3.1a) we have plotted (3.25) for $r = r_{crit}$ and $r = \infty$. Because all solutions to (3.23) which are bounded at $r = 0$ are linear multiples of the solution seen in figure (3.1b) the unstable fixed point must correspond to a solution which is not bounded at $r = 0$ and thus not in $L^2_r(\mathbb{R}_+;\mathbb{R})$. Note that if $\theta(r_{crit}) > \theta_{crit} \sim 2.7971$ then $\theta \to \frac{5\pi}{4}$ as $r \to \infty$. Numerically $\theta > \pi \; \forall \; r > 0$, so we are never even close to the unstable manifold.

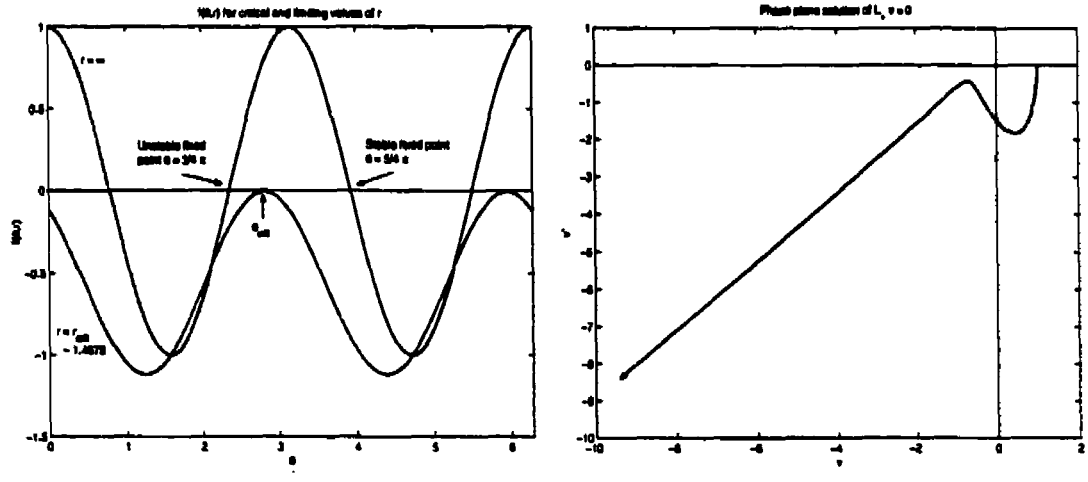

(a) $f(\theta, r)$ for r_{crit} and r_∞.

(b) Solution in the (v, v') plane.

Figure 3.1: Phase plane analysis of $\mathcal{L}_+ v = 0$.

Because we can solve (3.18) - (3.20), the solvability condition, $\int_0^\infty Rprdr = 0$, applied to (3.15) yields a differential equation for $L(t)$

$$\int_0^\infty \left(g\beta_\zeta + \epsilon h_\zeta + (L^2 l)_\zeta + L^2(1 + \gamma \sin 2S)R + \epsilon L^3 \Im\left(F(\psi_R)e^{-iS}\right)\right) Rrdr = 0. \tag{3.27}$$

In the following sections we simplify and analyze (3.27).

3.2.2 Useful Integrals

In order to apply the lemma from the previous section we need to evaluate integrals involving R, Rg, Rh and Rl. We begin with identities for the Townes soliton. Taking the inner product of (3.6)

with rR'

$$0 = (\nabla^2 R + R^3 - R, rR') = \int_0^\infty (rR')(rR')' dr + \int_0^\infty R^3 R' r^2 dr - \int_0^\infty RR' r^2 dr,$$

and integrating by parts we obtain

$$\frac{1}{2}\int_0^\infty R^4 r dr = \int_0^\infty R^2 r dr. \tag{3.28}$$

Similarly, taking the inner product of (3.6) with R yields

$$0 = (\nabla^2 R + R^3 - R, R) = \int_0^\infty (rR')' R dr + \int_0^\infty R^4 r dr - \int_0^\infty R^2 r dr,$$

using (3.28), and integrating by parts we derive

$$\int_0^\infty (R')^2 r dr = \int_0^\infty R^2 r dr. \tag{3.29}$$

Because the equations (3.18) - (3.20) all have a similar form, we consider the following general lemma.

Lemma 3 *For $c \in L^2_r$, if f solves*

$$\mathcal{L}_+ f = c$$

then f satisfies

$$\int_0^\infty Rf\, r\, dr = \int_0^\infty c(R + R'r)\, r\, dr.$$

PROOF. Direct calculation shows that

$$\mathcal{L}_+(R + R'r) = 2R$$

thus

$$2(f, R) = (f, \mathcal{L}_+(R + R'r))$$

however, $\mathcal{L}_+$ is self-adjoint, hence

$$\begin{aligned} 2(f, R) &= (\mathcal{L}_+ f, R + R'r) \\ &= (c, R + R'r) \end{aligned}$$

or,

$$\int_0^\infty Rf\, r\, dr = \frac{1}{2}\int_0^\infty c(R + R'r) r\, dr.$$

★

Even though we cannot solve (3.18) - (3.20) exactly, with this lemma in hand we are well on our way to writing down a modulation equation from the condition (3.27) because all that is required are integrals of the solutions to (3.18) - (3.20) and R.

Using lemma 3 with $c = -\frac{1}{4}R\rho^2$ and $f = g$ we have

$$\begin{aligned}\int_0^\infty Rg\rho\,d\rho &= \frac{1}{2}\int_0^\infty c(R+R'\rho)\rho\,d\rho \\ &= -\frac{1}{8}\int_0^\infty R(R+R'\rho)\rho\,d\rho \\ &= \frac{1}{8}\int_0^\infty R^2\rho^3\,d\rho\end{aligned}$$

Similarly, with $c = (a+\gamma\cos(2S))R$ and $f = l$ we have

$$\int_0^\infty Rl\rho\,d\rho = \frac{1}{2}\int_0^\infty (a+\gamma\cos(2S))(R^2+RR'\rho)\rho\,d\rho. \tag{3.30}$$

Lastly, taking $c = -L^3\Re\left(F\left(\frac{R}{L}e^{iS}\right)e^{-iS}\right)$ and $f = h$ we have

$$\int_0^\infty Rh\rho\,d\rho = -\frac{1}{2}L^3\int_0^\infty \Re\left(F\left(\frac{R}{L}e^{iS}\right)e^{-iS}\right)(R+R'\rho)\rho\,d\rho \tag{3.31}$$

for any perturbation F. There is still much calculation to be done, but all the heavy lifting is complete. We are ready to state the evolution equation for the modulation parameter $L(t)$.

3.3 Modulation equations

Recognizing that $\frac{\partial}{\partial\zeta} = L^2\frac{\partial}{\partial t}$, we can evaluate each term in (3.27) (see Appendix A) to obtain an ordinary differential equation for β. Combining this with the definition $\beta = -L^3L_{tt}$, we have a system of equations describing the evolution of the modulational scaling factor, L

$$\begin{aligned}L_{tt} &= -\frac{\beta}{L^3} \\ \beta_t &= \epsilon\frac{I_1}{I_2}\frac{L_t}{L^3} - \frac{N_c}{I_2} - \frac{\gamma}{I_2}\left(\left(1+\frac{L^2L_t^2}{2}\right)J_1 + 2J_3 + \left(L^2L_t^2-\beta\right)\left(\frac{1}{4}J_2 + \frac{LL_t}{8}J_4\right)\right),\end{aligned} \tag{3.32}$$

where the constants above are given by

$$\begin{aligned}N_c &= \textstyle\int_0^\infty R^2\rho\,d\rho && = 1.8612 \\ I_1 &= \frac{1}{I_2}\left(3N_c + \frac{2}{3}\int_0^\infty R^6\rho\,d\rho - \int_0^\infty (RR')^2\rho\,d\rho - \int_0^\infty R(R')^3\rho^2\,d\rho\right) && = 43.1789 \\ I_2 &= \tfrac{1}{8}\textstyle\int_0^\infty R^2\rho^3\,d\rho && = .2764\end{aligned}$$

and the functions J_n by

$$J_1 = \int_0^\infty \sin(2S)\, R^2 \rho\, d\rho \qquad |J_1| \le N_c$$
$$J_2 = \int_0^\infty \cos(2S) R^2 \rho\, d\rho \qquad |J_2| \le N_c$$
$$J_3 = \int_0^\infty \cos(2S) R^2 \rho^3\, d\rho \qquad |J_3| \le 8 I_2.$$

Recall that

$$S = \zeta + \frac{L L_t \rho^2}{4},$$
$$\zeta_t = \frac{1}{L^2}$$

so (3.32) is really a nonlinear integro-differential equation with the integral term $\frac{1}{L^2}$ buried in integrals of trigonometric functions.

A number of things can be gleaned about these ODE's before we attempt to integrate them. First notice that the dispersion coefficient a does not appear in (3.32) as it multiplies a conservative term. Also notice that the unpleasant terms involving the integrals J_n all arise due to the forcing term. Inspection of (3.32) shows that there are no steady states, that is there is no combination of L and β such that L_{tt}, L_t and β_t are all zero. Now, lets consider two special cases.

3.3.1 Unperturbed blow-up

For PNLS, $\epsilon = 0$, and as $L \to 0$ we have that $\beta_t \sim -\frac{N_c}{I_2}$. Here we have assumed that the integral terms, J_i, are adequately oscillatory (they contain $\cos\left(\int \frac{1}{L^2}\right)$) to be neglected. This reduced system

$$\begin{aligned} L_{tt} &= -\frac{\beta}{L^3} \\ \beta_t &= -\frac{N_c}{I_2} \end{aligned} \tag{3.33}$$

can then be solved. Integrating the second equation of (3.33) gives

$$\beta = \beta_0 - \frac{N_c}{I_2} t.$$

Assuming that $\lim_{t \to t^*} \frac{L}{\beta} = 0$, then near the blow-up time t^* we can approximate, $\beta \sim \beta^*$ with

$$\beta^* = \beta_0 - \frac{N_c}{I_2} t^*.$$

Now we can solve the first equation of (3.33)

$$L_{tt} = -\frac{\beta^*}{L^3}$$
$$L = \frac{\sqrt{t^* - t}}{2\sqrt{\beta^*}}$$

where t^* is the unknown blow-up time. This is a reasonable estimate and is similar to the rates previously calculated by Malkin [20] and Fibich [19] for blow-up in NLS. Inspection of figure (2.5) shows that this rate is sensible but too slow. A more detailed analysis shows [19] that the rate of blow-up for NLS is actually

$$L \sim A\sqrt{\frac{\log|\log(t^*-t)|}{t^*-t}}.$$

As was seen in section (2.4) this appears to be the correct rate for PNLS also. This logarithmic correction is very subtle and was obtained many years after the initial work of Fibich, Malkin, Papanicolau and others. It requires a detailed analysis of the matching of the central pulse ϕ_s to the distant small amplitude solution ϕ_{rad}. This rate is obtained by adding a correction term to (3.10), working in a dimension, d, greater than 2 and taking the limit $d \to 2^+$. It is not clear what, if any, effect the conjugate term in PNLS has on the rate of blow-up. A detailed numerical study of this effect has yet to be undertaken.

3.3.2 Saturating blow-up

In the case where $\epsilon > 0$ and $L \ll 1$ we can ignore all but the first term and consider

$$\begin{aligned} L_{tt} &= -\frac{\beta}{L^3} \\ \beta_t &= \epsilon k_1 \frac{L_t}{L^3} \end{aligned} \tag{3.34}$$

where $k_1 > 0$ not related to k_1 above. Integrating the second equation in (3.34) gives

$$\beta = -\frac{\epsilon k_1}{2}\frac{1}{L^2} + k_2,$$

with $k_2 > 0$. Using this definition for β in the first equation in (3.34) determines an ODE for L

$$L_{tt} = \frac{\epsilon k_1}{2}\frac{1}{L^5} - \frac{k_2}{L^3}. \tag{3.35}$$

which permits a Hamiltonian formulation with energy

$$\mathcal{H}(L, L_t) = \frac{1}{2}L_t^2 - \frac{\epsilon k_1}{8}\frac{1}{L^4} + \frac{k_2}{2}\frac{1}{L^2}$$

such that $\frac{d\mathcal{H}}{dt} = 0$. Writing (3.35) as a first order system

$$\frac{d}{dt}\begin{bmatrix} L \\ L_t \end{bmatrix} = \begin{bmatrix} L_t \\ \frac{\epsilon k_1}{2}\frac{1}{L^5} - \frac{k_2}{L^3} \end{bmatrix}$$

we see that there is one fixed point

$$(L, L_t) = \left(\sqrt{\frac{\epsilon k_1}{2k_2}}, 0\right),$$

which from the Hamiltonian formulation is clearly a center. At this stage we could calculate the period and the magnitude of oscillations given k_2 and $\mathcal{H}_0$. However, neither $\mathcal{H}_0$ nor k_2 is known a priori and neither may determined from the PDE. Instead we will take comfort that $||\phi||_\infty = \frac{1}{L_{\min}}$ scales no worse than $\sqrt{\epsilon}$.

Truly we do not have a Hamiltonian system; adding in just the dissipative term from (3.32) we consider

$$\begin{aligned} L_{tt} &= -\frac{\beta}{L^3} \\ \beta_t &= \epsilon k_1 \frac{L_t}{L^3} - \frac{N_c}{I_2}. \end{aligned} \tag{3.36}$$

Integrating the second equation of (3.36) and using the definition of β gives the forced equation

$$L_{tt} = \frac{\epsilon k_1}{2}\frac{1}{L^5} - \frac{k_2 - k_3 t}{L^3}. \tag{3.37}$$

Hence there exists a time t^* such that $t > t^* \Rightarrow L_{tt} > 0$, which implies $\lim_{t\to\infty} L = \infty$.

3.3.3 Comparison of SPNLS and quintic NLS

It is worthwhile to note that the quintic NLS equation

$$i\phi_t + |\phi|^2\phi + \nabla^2\phi - \epsilon|\phi|^4\phi = 0$$

gives, to leading order, the same modulation equations as above,

$$\begin{aligned} L_{tt} &= -\frac{\beta}{L^3} \\ \beta_t &= \epsilon k \frac{L_t}{L^3} \end{aligned}$$

with $k > 0$. Quintic NLS is known to exhibit saturating blow-up in the limit $\epsilon \to 0^+$ [17]. In fact, returning to SPNLS,

$$i\phi_t(1 + 2\epsilon|\phi|^2) + \nabla^2\phi(1 + \epsilon|\phi|^2) + |\phi|^2\phi + (i - a)\phi - \gamma\phi^* + \epsilon(\phi_r)^2\phi^* = 0.$$

dividing through by $(1 + 2\epsilon|\phi|^2)$ and then expanding in powers of ϵ, to $\mathcal{O}(\epsilon)$ we find

$$i\phi_t + \nabla^2\phi + |\phi|^2\phi + (i - a)\phi - \gamma\phi^* + \epsilon((\phi_r)^2\phi^* - 2|\phi|^4\phi - |\phi|^2\nabla^2\phi) = 0. \tag{3.38}$$

Certainly this is suggestive of the quintic NLS but the effect of the additional derivative terms is not immediately evident. But, after calculating the contribution of these different perturbations, it is evident that near blow-up SPNLS is, to leading order, indistinguishable from the saturating quintic NLS equation. Because this method is applicable to a broad variety of perturbations it is simple to compare SPNLS to other equations, such as the quintic NLS or equation (3.38). Presented in table (3.1) is a comparison of the contributions of 3 different perturbations which are seen to be very similar in the modulational context.

Equation	Perturbation	Coefficient of $\epsilon\frac{L_1}{L}$
SPNLS	$F = 2i\lvert\phi\rvert^2\phi_t + \lvert\phi\rvert^2\nabla^2\phi + (\phi_r)^2\phi^*$	43.1789
(3.38)	$F = -2\lvert\phi\rvert^4\phi - \lvert\phi\rvert^2\nabla^2\phi + (\phi_r)^2\phi^*$	42.1070
Quintic NLS	$F = -\lvert\phi\rvert^4\phi$	40.1582

Table 3.1: Comparison of perturbations.

3.4 Simulation of the modulation equations

One unfortunate fact about this modulational approach is that it provides only intermediate asymptotics. That is, given an arbitrary initial condition one cannot immediately predict its evolution. Instead we have a method to examine limiting behaviour assuming a number of conditions are reached. The full PDE problems considered in this problem are very complex and do not easily permit a simple reduction. It is perhaps surprising that any agreement is achieved between the modulation equations and the full PDEs at all - any agreement is only qualitative. The modulation equations predict blow-up when the PDEs blow-up and saturation when the PDEs saturate. However, in the saturation regime, the amplitudes, periods and attenuation factors agree at best to an order of magnitude. In figure (3.1) we provide some typical solutions of (3.2).

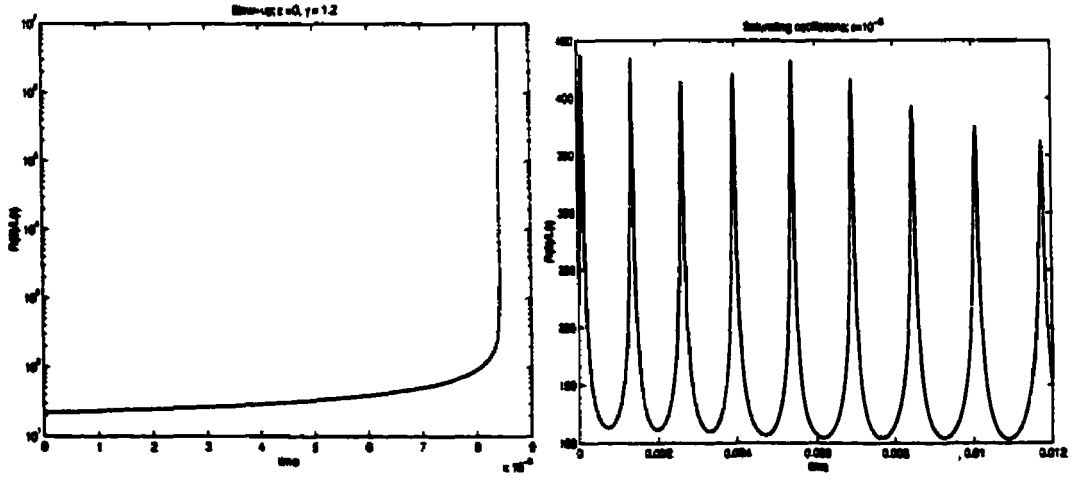

Figure 3.2: Integration of the modulation equations.

3.5 Convergence of higher order approximations to OPO

We now find conditions on the amplitude, L, such that the asymptotic expansion for W is convergent. It is important to recognize that even an exact solution for W still yields an equation which is only an approximation to OPO as we have assumed that $V(r,0)$ is found, when it is really prescribed.

For an approximate solution to OPO of the form

$$U = \frac{\phi}{\sqrt{\epsilon}} \quad V = \sum_{n=0}^{N} \epsilon^n W_n(\phi)$$

we have an evolution equation for ϕ

$$i\phi_t + |\phi|^2\phi + \nabla^2\phi + (i-a)\phi - \gamma\phi^* + \phi^* \sum_{n=1}^{N} \epsilon^n V_n = 0$$

where

$$W_0 = i(\phi^2 - \gamma) \quad W_n = i\frac{\partial}{\partial t} W_{n-1} + \frac{1}{2}\nabla^2 W_{n-1} + ia W_{n-1} \quad n > 1.$$

Assuming that we are near focusing then the amplitude, $\frac{R(0)}{L}$, is sufficiently large that the corrections to PNLS are important we write $L = \epsilon^p$ so that

$$|\phi| \sim \frac{1}{\epsilon^p} \quad p > 0.$$

From the temporal and spatial scalings derived in section (3.2) we see that

$$\phi_t \sim \frac{1}{\epsilon^{3p}}, \quad |\phi|^2\phi \sim \frac{1}{\epsilon^{3p}}, \quad \nabla^2\phi \sim \frac{1}{\epsilon^{3p}}, \quad (i-a)\phi \sim \frac{1}{\epsilon^p},$$
$$\gamma\phi^* \sim \frac{1}{\epsilon^p}, \quad W_0 \sim \frac{1}{\epsilon^{2p}}, \quad \text{and} \quad W_n \sim \frac{1}{\epsilon^{2p}} W_{n-1}$$

thus

$$\phi^* \epsilon^n W_n \sim \frac{1}{\epsilon^{p(2n+3)-n}}.$$

The relative importance of each additional corrective term is (multiplying through by ϵ^{3p})

$$\frac{\epsilon^n \phi^* W_n}{|\phi^2|\phi} \sim \epsilon^{(1-2p)n}.$$

Hence, as $\epsilon \to 0^+$ or as the solution focuses, each additional correction becomes less important and we are led to believe that even in saturating blow-up the expansion (1.20) converges, given that $L(0) \gg \epsilon^{\frac{1}{2}}$ and that all the derivatives of ϕ remain bounded. Furthermore, if $L(0) \gg \epsilon^{\frac{1}{2}}$ we would expect $L(t) \gg \epsilon^{\frac{1}{2}}$ for all time.

Chapter 4

Numerical methods

In this thesis 5 distinct numerical problems have been considered

1. Integration of smooth solutions to OPO and PNLS in 1 and 2 dimensions.
2. Integration of blow-up solutions to OPO and PNLS in 2 dimensions with radial symmetry.
3. Generating the Townes soliton profile over all space.
4. Evaluating integrals over all space of powers of the Townes soliton, it's radial derivative and the spatial coordinate.
5. Integrating the modulation equations.

The first two problem posed the most challenge, demanded the most effort and were the most instructive - a brief discussion of the last three problems is included for completeness.

4.1 The split-step Fourier method

Split-step methods are used to solve a wide variety of problems which take the form

$$\begin{aligned} u_t &= \mathcal{L}_1(u) + \mathcal{L}_2(u) \\ u(0) &= u_0 \end{aligned} \tag{4.1}$$

That is evolution equations with two (or more) distinct characters such that the separate problems

$$v_t = \mathcal{L}_1(v) \qquad \text{and} \qquad w_t = \mathcal{L}_2(w)$$

are much easier to solve independently. This type of splitting can be dimensional (as is often seen in fluid dynamics problems [22]), with the simplest example being

$$\mathcal{L}_1 = \frac{\partial}{\partial x} \quad \text{and} \quad \mathcal{L}_2 = \frac{\partial}{\partial y}.$$

Or the splitting might be done into linear and non-linear parts to exploit the easy solution of the linear piece - as has been done in this thesis. The method of solution then proceeds by solving the separate problems sequentially. Formally denoting the solutions to the sub-problems as

$$v(t) = e^{\int_0^t \mathcal{L}_1} v(0) \quad w(t) = e^{\int_0^t \mathcal{L}_2} w(0)$$

then a solution over one time step, Δt would be obtained in the following manner

$$u_{\frac{1}{2}} = e^{\Delta t \mathcal{L}_1} u_0$$
$$u(\Delta t) = e^{\Delta t \mathcal{L}_2} u_{\frac{1}{2}}.$$

When using any splitting method we introduce a splitting error; this is an error due strictly to the splitting and cannot be overcome by solving the sub-problems more accurately. When the operators $\mathcal{L}_1, \mathcal{L}_2$ commute then this method introduces no splitting error. Otherwise, it introduces a first-order splitting error. A better splitting due to Strang introduces a second-order splitting error - as we shall see. For the problems under consideration here an n-th order error is one proportional to $(\Delta t)^n$, where Δt is the time-step.

4.1.1 The split-step Fourier method for NLS-type equations

Both the OPO (1.11) and PNLS (2.1) equations may be written in the form

$$i\mathbf{v}_t + \nabla^2 \mathbf{v} + a\mathbf{v} + \mathbf{N}(\mathbf{v}) + \mathbf{F} = 0 \tag{4.2}$$

where the vector $\mathbf{v} = u$ in the case of PNLS and $\mathbf{v} = (U, V)$ for OPO. $\mathbf{N}$ is the appropriate non-linearity and $\mathbf{F}$ is the constant forcing term. When smooth in time and space over the time period of interest, problems of this type are amenable to the split-step Fourier method. The method and its analysis are identical for both OPO and PNLS, but for the sake of both brevity and clarity only PNLS will be discussed. Splitting into linear and non-linear pieces, we can solve PNLS via the sub-problems

$$iv_t + \nabla^2 v + (i - a)v = 0 \tag{4.3}$$
$$iw_t - \gamma w^* + |w|^2 w = 0. \tag{4.4}$$

This splitting is advantageous for two reasons: the linear equation (4.3) can be solved exactly and the non-linear equation contains no spatial derivatives. This second point is particularly important

because it means that the splitting does not introduce any errors related to boundary conditions. Equation (4.3) may be solved exactly by taking the Fourier transform (hence the name)

$$\begin{aligned} \hat{v} &= \mathcal{F}[v] \\ i\hat{v}_t - (k^2 - i + a)\hat{v} &= 0 \\ \hat{v}(t) &= e^{-t(1+i(k^2+a))}\hat{v}(0) \\ \text{or} \quad v(t) &= \mathcal{F}^{-1}\left[e^{-t(1+i(k^2+a))}\mathcal{F}[v(0)]\right]. \end{aligned} \tag{4.5}$$

Because it contains no spatial derivatives, (4.4) may be solved with your favourite time integrator. All calculations presented in this thesis were done using the fourth-order Runge-Kutta method.

4.1.2 The Strang splitting

Solving each of (4.3) and (4.4) sequentially over a full time-step Δt yields a method that is first order accurate in time when at least a first order method is used to solve (4.4). A more intelligent splitting, due to Strang [23], involves solving one problem over half a time-step on either side of solving the second problem. Returning to the notation of the model problem above, we would have

$$\begin{aligned} u_{\frac{1}{3}} &= e^{\int_0^{\frac{\Delta t}{2}} \mathcal{L}_1} u_0 \\ u_{\frac{2}{3}} &= e^{\int_0^{\Delta t} \mathcal{L}_2} u_{\frac{1}{3}} \\ u(\Delta t) &= e^{\int_0^{\frac{\Delta t}{2}} \mathcal{L}_1} u_{\frac{2}{3}}. \end{aligned}$$

Writing the exact solution to (2.1) as $u = f + ig$ for real-valued functions f and g and the approximate solution as the vector $\mathbf{u} = (f_1, g_1, f_2, g_2, ..., f_N, g_N)$, where $u_j = (f_j, g_j)$ is the approximate solution at $x = n\,\Delta x$, we can write our problem in the form

$$\mathbf{u}_t = (A + B(\mathbf{u}))\mathbf{u} \tag{4.6}$$

where A is the $2N$ by $2N$ matrix representation of the solution to (4.5) and B is composed of N 2×2 blocks along the diagonal with the j-th block having the form

$$B_j = \begin{bmatrix} -g_j f_j & -\gamma - g_j^2 \\ -\gamma + f_j^2 & f_j g_j \end{bmatrix}$$

Because PNLS has the form (4.6), it is useful to consider the following lemma.

Lemma 4 *Given a system of ordinary differential equations of the form*

$$\mathbf{u}_t = (A + B(\mathbf{u}))\,\mathbf{u},$$

where A and B are square matrices with A constant and B continuous in all its arguments and initial data

$$\mathbf{u}(0) = \mathbf{u}_0.$$

the solution at $t = \Delta t$ by the Strang-splitting

$$\mathbf{U} = e^{\frac{\Delta t}{2}A}\mathbf{w} \tag{4.7}$$

where $\mathbf{w}$ is the solution at $t = \Delta t$ of

$$\begin{aligned}\mathbf{w}_t &= B(\mathbf{w})\mathbf{w}\\ \mathbf{w}(0) &= e^{\frac{\Delta t}{2}A}\mathbf{u}_0.\end{aligned}$$

is second order accurate in time. That is, the local difference between the approximate solution $\mathbf{U}_1$ and the exact solution $\mathbf{u}(\Delta t)$ can be bounded

$$\|\mathbf{U} - \mathbf{u}(\Delta t)\| < k\Delta t^3$$

for some k independent of time.

PROOF. Given initial data at time $t = 0$ we solve for $\mathbf{U}$ the approximate solution to (4.6) at time $t = \Delta t$ in the following manner

$$\mathbf{u}^* = e^{A\frac{\Delta t}{2}}\mathbf{u}_0 \tag{4.8}$$

$$\mathbf{u}^{**} = (I - \frac{\Delta t}{2}B^{**})^{-1}(I + \frac{\Delta t}{2}B^*)\mathbf{u}_0 \tag{4.9}$$

$$\mathbf{U} = e^{A\frac{\Delta t}{2}}\mathbf{u}^{**} \tag{4.10}$$

Where

$$\begin{aligned}B^* &= B(\mathbf{u}^*)\\ B^{**} &= B(\mathbf{u}^{**})\end{aligned}$$

To understand the convergence properties of this splitting, we need to compare the approximate solution $\mathbf{U}$ to $\mathbf{u}_1 = \mathbf{u}(\Delta t)$. We can solve (4.6) formally by integrating

$$\mathbf{u}_1 - \mathbf{u}_0 = \int_{t_0}^{t_1}(A + B(\mathbf{u}))\,\mathbf{u}ds. \tag{4.11}$$

Denoting

$$\begin{aligned}B_0 &= B(\mathbf{u}_0)\\ B_1 &= B(\mathbf{u}_1)\end{aligned}$$

and approximating the integral in (4.11) with the trapezoid rule we find an implicit representation for $\mathbf{u}_1$

$$\begin{aligned} \mathbf{u}_1 - \mathbf{u}_0 &= \frac{\Delta t}{2}((A+B_1)\,\mathbf{u}_1 + (A+B_0)\,\mathbf{u}_0) + (\Delta t)^3\,\mathbf{e}_0 \\ \mathbf{u}_1 &= (I - \frac{\Delta t}{2}(A+B_1))^{-1}(I + \frac{\Delta t}{2}(A+B_0))\,\mathbf{u}_0 + (\Delta t)^3\,\mathbf{e}_1 \end{aligned} \tag{4.12}$$

where $\mathbf{e}_i$ are errors whose magnitude is independent of Δt. In all further calculations, e will indicate an arbitrary error vector with magnitude independent of Δt. The local truncation error

$$\mathbf{E} = \mathbf{u}_1 - \mathbf{U}, \tag{4.13}$$

is defined as the difference between the exact and approximate solutions at $t = \Delta t$. It is our goal to show that $|\mathbf{E}| \sim \mathcal{O}(\Delta t)^3$. Because $\mathbf{u}_1$ has only been calculated to $\mathcal{O}(\Delta t)^3$, all terms on this order will be lumped into an unknown vector e. The only thing known about e is that it is independent of Δt. Showing that it is truly order 1 will require a more involved analysis for each particular A, B and $\mathbf{u}_1$. It is in this subsequent analysis that any time-step restrictions will be made apparent. For now, it is assumed Δt has been chosen such that all the formal manipulations are legitimate.

Expanding (4.13) using (4.11) - (4.10) we have

$$\begin{aligned} \mathbf{u}_1 - \mathbf{U} = [&\left(I - \frac{\Delta t}{2}(A+B_1)\right)^{-1}\left(I + \frac{\Delta t}{2}(A+B_0)\right) \\ &- e^{A\frac{\Delta t}{2}}\left(I - \frac{\Delta t}{2}B^{**}\right)^{-1}\left(I + \frac{\Delta t}{2}B^{*}\right)e^{A\frac{\Delta t}{2}}]\,\mathbf{u}_0 + (\Delta t^3)\,\mathbf{e} \end{aligned}$$

$$\begin{aligned} \mathbf{u}_1 - \mathbf{U} = [&\frac{\Delta t}{2}(B_0 + B_1 - B^{*} - B^{**}) + \frac{\Delta t^2}{4}((A+B_1)(B_0+B_1) \\ &- B^{**}(B^{**} + B^{*} + A) - A(B^{*} + B^{**}) - (B^{*} + B^{**})\,A)]\,\mathbf{u}_0 + (\Delta t)^3\mathbf{e} \end{aligned}$$

This leaves two equations which require more careful consideration. At $\mathcal{O}(\Delta t)$ we have

$$\begin{aligned} (B_0 - B^{*} + B_1 - B^{**})\mathbf{u}_0 &= (2B_1 - 2B^{**} + \nabla B_1(\mathbf{u}_1 - \mathbf{u}_0) - \nabla B^{**}(\mathbf{u}^{**} - \mathbf{u}^{*}))\,\mathbf{u}_0 + \Delta t^2\,\mathbf{e} \\ &= -2\nabla B_1(\mathbf{u}_1 - \mathbf{U}) + \nabla B_1(\mathbf{u}_1 - \mathbf{u}_0 - \mathbf{u}^{**} - \mathbf{u}^{*}) + |\mathbf{E}|^2\,\mathbf{e}_1 + \Delta t^2\,\mathbf{e}_2 \end{aligned}$$

Recalling (4.9) - (4.13) we have that

$$\begin{aligned} \mathbf{u}_1 - \mathbf{u}^{**} &= \mathbf{u}_1 - e^{-\frac{\Delta t}{2}A}\mathbf{U} \\ &= \mathbf{E} + \frac{\Delta t}{2}A\,\mathbf{U} + \Delta t^2\,\mathbf{e} \\ \mathbf{u}_0 - \mathbf{u}^{*} &= \mathbf{u}_1 - e^{\frac{\Delta t}{2}A}\mathbf{u}_0 \\ &= -A\frac{\Delta t}{2}\mathbf{u}_0 + \Delta t^2\,\mathbf{e} \\ &= -A\frac{\Delta t}{2}\mathbf{u}_1 + \Delta t^2\,\mathbf{e} \end{aligned}$$

thus,

$$(B_0 - B^* + B_1 - B^{**})\mathbf{u}_0 = (-2\nabla B_1(\mathbf{E}) + \nabla B_1((I - \frac{\Delta t}{2}A)\mathbf{E}))\mathbf{u}_0 + \Delta t^2 \mathbf{e}$$
$$= -\nabla B_1(I + \frac{\Delta t}{2}A)\mathbf{E} + \Delta t^2 \mathbf{e}.$$

At $\mathcal{O}(\Delta t)^2$ we have

$$(A + B_1)(B_0 + B_1) - B^{**}(B^{**} + B^* + A) - A(B^* + B^{**}) - (B^* + B^{**})A$$
$$= A(B_0 - B^*) + A(B_1 - B^{**}) + (B_1 B_0 - B^{**} B^*)$$
$$+ (B_1^2 - (B^{**})^2) + (2B_1 - (B^* + B^{**}))A.$$

But, from the definitions of the B matrices, the norm of each of these differences is $\mathcal{O}(\Delta t)$. Thus

$$|\mathbf{E}| \leq \Delta t\,|\nabla B_1|\,|I + \frac{\Delta t}{2}A|\,|\mathbf{E}|\,|\mathbf{u}_0| + \Delta t^3\,|\mathbf{e}|$$

As, $|\nabla B_1|, |A|, |\mathbf{u}_0|, |\mathbf{e}|$ are all independent of Δt we have that

$$|\mathbf{E}| \leq k\,\Delta t^3 \tag{4.14}$$

for some real number k. k will be dependent on $A, B, \mathbf{u}_0$ and how (4.9) is approximated. ★

4.1.3 The split-step Fourier method in practice

The Strang splitting is particularly useful for this problem as the two Fourier transforms at the end of one step and beginning of the next can be collapsed together

$$\mathcal{F}^{-1}\left[e^{-\frac{\Delta t}{2}(1+i(k^2+a))}\mathcal{F}\left[\mathcal{F}^{-1}\left[e^{-\frac{\Delta t}{2}(1+i(k^2+a))}\mathcal{F}[\mathbf{U}_n]\right]\right]\right] = \mathcal{F}^{-1}\left[e^{-\Delta t(1+i(k^2+a))}\mathcal{F}[\mathbf{U}_n]\right].$$

This explains why this method enjoys such wide use; a 2nd-order method in time with spectral accuracy in space is obtained for the price of a first order method in time. The work is on the order of $\mathcal{O}(n\log(n))$ floating point operations work per time-step to solve a nonlinear parabolic problem, with a very generous stability constraint.

To achieve second-order accuracy we need to solve the nonlinear problem with at least a 2nd order method. A higher order method may at first seem wasteful because we will never surpass the second order splitting error, but higher order methods are also often more accurate. Through a process of trial and error it was determined that a fourth-order Runge-Kutta step was well-suited for the problems under consideration. Any method higher than second order results in primarily splitting error. A third-order Runge-Kutta method also works well, with a marginal speed gain over

the fourth order method. Higher order methods require more work and provided no visible benefit. Lower order methods, while cheaper, require a smaller step size for comparable accuracy and may turn out to be more costly overall. This situation depends upon the FFT algorithm used - a faster FFT would reduce the cost of the increased steps and make a lower order method such as midpoint more desirable. Another attractive aspect of this method is that the most work intensive aspect of each step, the FFT, is naturally parallelizable.

All problems were solved on a physical grid $x \in [-L, L - \Delta x]$ where $\Delta x = \frac{2L}{2^n}$ for an integer n. For computations presented in this thesis typically $n = 10$ was used with $\Delta t \leq .005$ and $L = 20$. Periodic boundary conditions were used to fully exploit the speed of the discrete Fourier transform.

To test the convergence properties of the method, we considered the following one dimensional model problem

$$i\phi_t + ic\phi_x + \phi_{xx} + |\phi|^2\phi + (i-a)\phi - \gamma\phi^* = 0$$
$$\phi(0,x) = \phi_+(x).$$

This problem has the exact solution

$$\phi(x,t) = \phi_+(x - ct),$$

with ϕ_+ as given by (2.6).

Presented in tables (4.1) and (4.2) are convergence results for the test problem when using 2^{11} modes for the discrete Fourier transform. From these tables we can clearly see the 2nd order convergence as halving the time-step results consistently in reducing the error by a factor ~ 4. It is also clear that the RK4 method is more accurate for this problem than the midpoint method and that the midpoint method is unstable for the largest time-step, $dt = .4096$. For all runs the parameters $a = 1$, $\gamma = 1.2$ and $c = 2$ were used. Solutions were integrated from $t = 0$ to $t = 10.24$ on a physical domain $x \in [-40, 40]$. The rate is computed as

$$Rate_n = \log_2\left(\frac{error_n}{error_{n+1}}\right).$$

The cpu times quoted are for a Sun UltraSparc5.

All of the above comments of course also to 2 space dimensions, except instead of operations on vectors we have operations on matrices. In 2D, especially for OPO, using midpoint for the nonlinear term becomes more attractive when using many modes as it has a smaller memory requirement.

time-step	cpu time (s)	L^∞ error	L_2^2 error	rate
0.00010000	306.46922500	4.639613e-08	3.824585e-16	3.9985
0.00020000	152.00974700	1.854452e-07	6.112852e-15	4.0003
0.00040000	75.44252900	7.420137e-07	9.782635e-14	4.0010
0.00080000	37.98832700	2.970582e-06	1.566332e-12	4.0021
0.00160000	18.87134600	1.190276e-05	2.509735e-11	4.0040
0.00320000	9.50189400	4.777261e-05	4.026846e-10	4.0077
0.00640000	4.71509300	1.923509e-04	6.477285e-09	4.0137
0.01280000	2.37604900	7.789887e-04	1.046283e-07	4.0217
0.02560000	1.18103600	3.185265e-03	1.699476e-06	4.0245
0.05120000	0.59608700	1.319501e-02	2.765769e-05	3.9913
0.10240000	0.29687500	5.482162e-02	4.398699e-04	4.2219
0.20480000	0.14941400	3.084429e-01	8.207983e-03	-
0.40960000	0.07617200	∞	∞	-

Table 4.1: Errors with 2^{11} modes using the midpoint method.

time-step	cpu time (s)	L^∞ error	L_2^2 error	rate
0.00010000	484.11483400	1.447775e-08	4.138145e-17	3.9967
0.00020000	240.77233300	5.769912e-08	6.605954e-16	4.0053
0.00040000	119.91713600	2.309410e-07	1.057816e-14	4.0012
0.00080000	60.14365400	9.242028e-07	1.696386e-13	4.0033
0.00160000	29.97760500	3.699925e-06	2.726822e-12	4.0067
0.00320000	15.04738800	1.482379e-05	4.403033e-11	4.0132
0.00640000	7.49466800	5.947750e-05	7.171500e-10	4.0257
0.01280000	3.76171100	2.392064e-04	1.186753e-08	4.0486
0.02560000	1.87759800	9.646452e-04	2.015716e-07	4.0862
0.05120000	0.94314000	4.299738e-03	3.532291e-06	4.1312
0.10240000	0.47028700	2.025473e-02	6.197169e-05	3.9302
0.20480000	0.23632800	8.534018e-02	9.446841e-04	2.3238
0.40960000	0.11914100	1.994187e-01	4.729481e-03	-

Table 4.2: Errors with 2^{11} modes using the RK4 method.

4.2 Moving Mesh methods

Although accurate, simple, and fast, the split-step Fourier method cannot solve problems with blow-up. Without special re-gridding as the solution focuses, it is impossible to keep a reasonable resolution. A static rescaling of the problem near blow-up is possible but not nearly as efficient as dynamically adaptive methods. In the case of PNLS with $\phi_0 = 4e^{-r^2}$, $\gamma = 1.2$ which, as seen in figure (2.2), does not lead to blow-up, excellent agreement was achieved between integration with the split-step and moving mesh methods. Sadly, due to excessive temporal and spatial gradients no other cases could be reasonably compared.

For the blow-up and saturating blow-up problems the package MovCol [24] was used. The basic premise is to use the method of lines and require the spatial discretization to evolve with the solution by equidistributing a specified monitor function, $M(x,t)$ in the manner

$$\int_0^{x_i(t)} M(x,t)\,dx = \int_0^{L} M(x,t)\,dx.$$

This requires solving a PDE for the mesh as well as for the solution on that mesh. It is a lovely idea as it puts the grid points where they are required (provided you have a good monitor function!). Moving mesh methods have been employed successfully for many problems with blow-up [24, 25, 26] when fixed grids are wholly inadequate.

4.2.1 Choosing a monitor function

The key to moving mesh methods is in the choice of a proper monitor function.

Consider figure (4.1), what is most disturbing is that this figure shows the evolution of time of PNLS with the same initial condition, $\phi_0 = 5e^{-r^2}$, computed with sensible parameters and sensible monitor functions. In fact three of the monitor functions have been shown [26] to preserve the scaling invariances present in NLS near blow-up. Both $M = |\phi|$ and $M = \sqrt{|\phi|^4 + 2|\phi_r|^2}$ have been used successfully to compute self-similar blow-up solutions to NLS in [26]. From numerical experiments in appears that monitor functions with any radial derivative dependence can develop, (due to the influence of the conjugate term), a mesh disaster, that is too many points cluster in regions of small amplitude oscillation and then the solution is lost. In figure (4.2) we see the tracking of spurious oscillation near blow-up using an arclength monitor function for PNLS whereas for NLS this monitor function was able to follow blow-up in NLS until $|\phi| \sim 10^5$, at which point the time-integrator failed due to error tolerances and a smooth solution was returned.

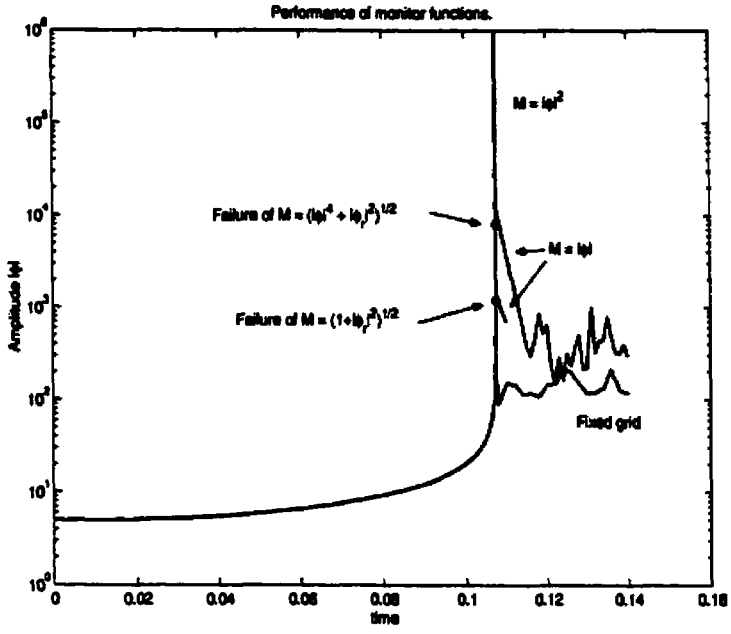

Figure 4.1: Comparison of monitor functions.

This highlights, for me, the great strength of adaptive methods - they not only focus on particular aspects of the solution but ignore others as well. The solution with $M = |\phi|^2$ simply did not see any radiation or noise. All computations in this thesis involving blow-up were generated using $M = |\phi|^2$. All saturating computations were done using $M = |\phi|$ which for a suitable number of mesh points was able to track blow-up solutions to $|\phi| \sim 10^4$ - well beyond the saturation level. $M = |\phi|$ was used because it was typically $10 - 20$ times faster for the same problem as $M = |\phi|^2$ due to the smaller grid spacing near the peak and the subsequent added stiffness.

4.2.2 Computational Parameters

Because both OPO and PNLS are noisier than NLS, and there was some concern about boundary effects, test problems were solved on the grids $r \in [0, L]$ with $L = 10, 20$ with both Dirichlet and Neumann conditions. One exception to this is for the V component of OPO where Neumann conditions were used exclusively. No significant difference was noticed between using Dirichlet or Neumann conditions for solutions with blow-up. For saturating blow-up and large values of ϵ, a difference can be seen when the solutions have melted enough that mass approaches the boundary. Because the problem has radial symmetry, all problems were solved with all components having a

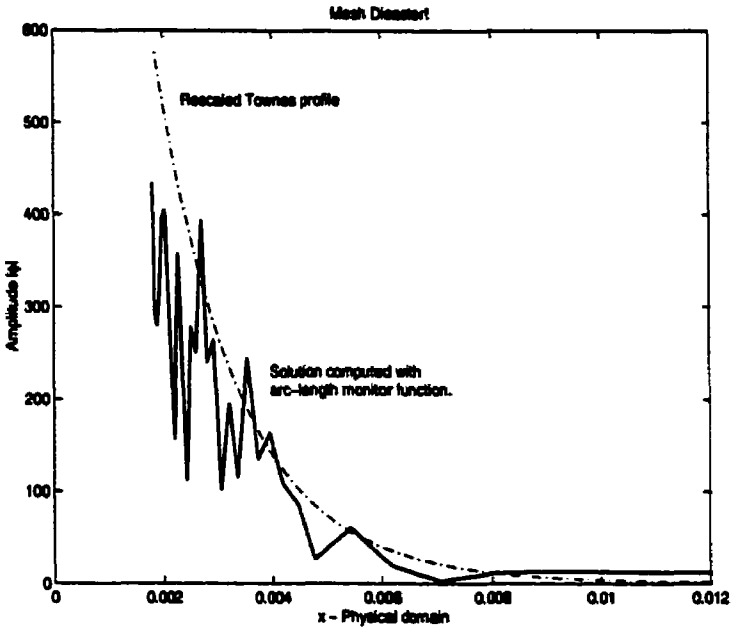

Figure 4.2: Spurious oscillation.

Neumann condition at the boundary. Solutions with blow-up were computed on $r \in [0, 10]$ and saturating solutions on $r \in [0, 20]$.

MovCol [25] is a highly customizable code with many user-specifiable parameters. In all runs the spatial smoothing parameter was taken to be $ip = 5$, the temporal smoothing was chosen $\tau = 10^{-4}$ and the relative tolerance for the time integration was chosen $rtol = 10^{-6}$. While a small absolute tolerance is desirable for accurate solutions, setting it too stringently can require an excessively small time-step near blow-up. The absolute tolerance, $atol$, was decreased as $|\phi|$ increased in the following way

$$atol = \begin{cases} 10^{-8} & \text{if } |\phi| \leq 10^4, \\ 10^{-6} & \text{if } 10^4 < |\phi| \leq 10^5 \\ 10^{-4} & \text{if } |\phi| > 10^5 \end{cases}$$

For the solutions without blow-up the tolerances were set: $rtol = 10^{-6}$, $atol = 10^{-8}$. For problems with blow-up, $N = 101$ spatial nodes were used and for saturating problems, $N = 141$. Adjustment of these parameters did not give rise to significantly different solutions.

4.3 Shooting the Townes

The Townes soliton which plays a central role in the theory of blow-up of the nonlinear Schrodinger equation can be stated as the solution to

$$R'' + \frac{1}{r}R' + R^3 - R = 0$$
$$R'(0) = 0$$
$$\lim_{r\to\infty} = 0$$
$$r < \infty \Rightarrow R(r) > 0, R'(r) < 0$$

Despite no closed form representation much is known about this solution, for instance for $r \gg 1 \Rightarrow$, $R \sim \frac{A_r}{\sqrt{r}e^r}$, where $A_r \sim 3.52$.

Formally the definition of R represents a boundary value problem, and with the asymptotic behaviour of R known, even a solvable one. However boundary value problem solvers are often delicate requiring a very good initial guess. To construct this guess a shooting method is often used. This turned out to be adequate. A shooting method was implemented in MatLab that continued the solution on increasingly larger intervals until a positive, monotonically decreasing solution was obtained on $r \in [0, 15]$. This was done by using a boundary condition based on the known asymptotic form of R and penalizing negative or increasing solutions. While this solution could then have been used for an initial guess for ColSys, this was deemed unnecessary as integrals of the solution agree exactly with published values.

4.4 Evaluation of integrals

In the modulation equations, numerous integrals involving powers of R, R' and r appear. The solution for R was returned by the integration routine onto a uniform grid on $[0, 10]$ and then extended using the asymptotic approximation to $[0, 20]$. Note that $R(20) \sim e^{-20}$. All integrals over all space were then evaluated numerically on this interval with $\Delta x = .01$ using the fourth order extended Simpson's rule. The extended Simpson's rule is derived from applying Simpson's three-point rule to non-overlapping pairs of intervals and takes the form

$$\int_{x_1}^{x_N} f(x)dx = \Delta x \left(\frac{1}{3}f_1 + \frac{4}{3}f_2 + \frac{2}{3}f_3 + \frac{4}{3}f_4 + ... + \frac{2}{3}f_{N-2} + \frac{4}{3}f_{N-1} + \frac{1}{3}f_N\right) + \mathcal{O}(\Delta x^4).$$

Here N is odd with $\Delta x = \frac{x_N - x_1}{N-1}$ and $f_n = f((n-1)\Delta x)$.

4.5 Integration of the modulation equations

The third order system (3.32), was re-written as a fourth-order system

$$\frac{d}{dt}\begin{bmatrix} L \\ L_t \\ \beta \\ \zeta \end{bmatrix} = \begin{bmatrix} L_t \\ -\frac{\beta}{L^3} \\ \epsilon \frac{I_1}{I_2}\frac{L_t}{L^3} - \frac{N_c}{I_2} - \frac{\gamma}{I_2}\left(\left(1+\frac{L^2L_t^2}{2}\right)J_1 + 2J_3 + \left(L^2L_t^2-\beta\right)\left(\frac{1}{4}J_2 + \frac{LL_t}{8}J_4\right)\right) \\ \frac{1}{L^3} \end{bmatrix} \tag{4.15}$$

and integrated with the built-in MatLab stiff ODE solver ode15s. This formulation hides the fact that we are really solving an integro-differential equation and introduces a need for the unknowable initial condition ζ_0. Fortunately, due to the oscillatory behaviour of the integrals J_n and the scale of the initial values for L, L_t and β, varying ζ_0 has little effect on the nature of solutions to (4.15).

Chapter 5

Conclusions and future work

Many questions have been raised in this thesis which suggest additional study. In the physics community it has long been understood that χ^2 materials provide damping. While this is certainly true when there is one dominant field present, as we have seen interactions can lead to a type of resonance that makes a χ^2 material behave as a χ^3 material. It would be interesting see how broad a phenomena this is mathematically and whether or not it can be observed physically.

The numerical investigations undertaken lead one to wonder about the differences between PNLS and NLS both leading to and at blow-up. Also there is work to be done in understanding the best way to integrate problems, such as PNLS, with only asymptotic scale invariances and to determine the true source and effect of the oscillatory radiation seen in the moving mesh calculations. Lastly, I am curious to know if there is an efficient way to rescale the problem in two dimensions to be able to integrate arbitrary data in two dimensions with the split-step FFT code.

Appendix A

Wherein we slay the beast that is the solvability condition

$$\int_0^\infty \left(g\beta_\zeta + \epsilon h_\zeta + (L^2 l)_\zeta + L^2(1+\gamma\sin 2S)R + \epsilon L^3 \Im\left(F(\psi_R)e^{-iS}\right)\right) R r dr = 0, \qquad \text{(A.1)}$$

where g, h and l come from the equations

$$\begin{aligned}
\mathcal{L}_+ g &= -\frac{1}{4}\rho^2 R, & g'(0) = 0, \quad & \lim_{\rho\to\infty} g = 0 \\
\mathcal{L}_+ h &= -L^3 \Re\left(F\left(\frac{R}{L}e^{iS}\right)e^{-iS}\right), & \tfrac{\partial h}{\partial \rho}(\zeta, \rho = 0) = 0, \quad & \lim_{\rho\to\infty} h = 0 \\
\mathcal{L}_+ l &= (a + \gamma\cos 2S)R, & \tfrac{\partial l}{\partial \rho}(\zeta, \rho = 0) = 0, \quad & \lim_{\rho\to\infty} l = 0,
\end{aligned}$$

and the perturbation F is given by

$$\begin{aligned}
F &= i|\phi|^2\phi_t + |\phi^2|\nabla^2\phi + \phi_r^2\phi^* \\
&\equiv F_1 + F_2 + F_3.
\end{aligned}$$

Recalling from lemma 3 that

$$\mathcal{L}_+ f = c \Rightarrow \int_0^\infty R f \rho\, d\rho = \frac{1}{2}\int_0^\infty c(R + R'\rho)\rho\, d\rho,$$

and recognizing that

$$\frac{\partial}{\partial\zeta} = L^2\frac{\partial}{\partial t},$$

we can begin evaluating (A.1) term by term.

$$\begin{aligned}
-\beta_\zeta \int_0^\infty gR\rho\, d\rho &= \frac{L^2\beta_t}{8}\int_0^\infty R(R + R'\rho)\rho\, d\rho \\
&= -\frac{L^2\beta_t}{8}\int_0^\infty R^2\rho^3\, d\rho \\
&\equiv -\frac{L^2\beta_t}{8} I_1
\end{aligned}$$

$$\begin{aligned}\int_0^\infty (1+\gamma\sin(2S))R^2\rho\,d\rho &= \int_0^\infty R^2\rho\,d\rho+\gamma\int_0^\infty \sin(2S)R^2\rho\,d\rho\\ &\equiv N_c+\gamma J_1\end{aligned}$$

$$\begin{aligned}L^2\frac{\partial}{\partial t}\int_0^\infty L^2 lR\rho\,d\rho &= \left(2L^3L_t+L^4\frac{\partial}{\partial t}\right)\int_0^\infty L^2 lR\rho\,d\rho\\ \int_0^\infty L^2 lR\rho\,d\rho &= \frac{1}{2}\int_0^\infty (a+\gamma\cos(2S))R(R+R'\rho)\rho\,d\rho\\ &= \frac{a}{2}\int_0^\infty R(R+R'\rho)\rho\,d\rho+\frac{\gamma}{2}\int_0^\infty \cos(2S)R(R+R'\rho)\rho\,d\rho\\ &= 0+\frac{\gamma}{2}\int_0^\infty \cos(2S)R^2\rho\,d\rho-\frac{\gamma}{2}\int_0^\infty \cos(2S)R^2\rho\,d\rho+\frac{\gamma}{2}\int_0^\infty \sin(2S)S_\rho R^2\rho\,d\rho\\ &= \frac{\gamma LL_t}{4}LL_t\int_0^\infty \sin(2S)R^2\rho^3\,d\rho\\ &\equiv \frac{\gamma LL_t}{4}LL_tJ_2\end{aligned}$$

$$\begin{aligned}\frac{\partial}{\partial t}(LL_tJ_2) &= \left(L_t^2+LL_{tt}\right)J_2+LL_t\frac{\partial}{\partial t}J_2\\ \frac{\partial}{\partial t}J_2 &= 2\int_0^\infty \cos(2S)R^2\rho^3\,d\rho+\frac{L_t^2+L_{tt}}{2}\int_0^\infty \cos(2S)R^2\rho^5\,d\rho\\ &\equiv \frac{2}{L^2}J_3+\frac{L_t^2+L_{tt}}{2}J_4\end{aligned}$$

Hence

$$\frac{\partial}{\partial t}\left(\int_0^\infty L^2 lR\rho\,d\rho\right) = \gamma\left(\frac{L^2L_t^2}{2}J_1+2J_3+(L^2L_t^2-\beta)\left(\frac{J_2}{4}+\frac{LL_t}{8}J_4\right)\right)$$

$$\frac{\partial}{\partial t}\left(\int_0^\infty hR\rho\,d\rho\right) = \frac{\partial}{\partial t}\left(-\frac{L^3}{2}\int_0^\infty \Re\left[Fe^{-ei\bar{S}}\right](R+R'\rho)\rho\,d\rho\right)$$

$$\begin{aligned}F &= 2i|\phi|\phi_t+|\phi|^2\nabla_r^2\phi+\phi_r^2\phi^*\\ &\equiv F_1+F_2+F_3\end{aligned}$$

F_1 :

$$\begin{aligned}
L^3\int_0^\infty \Re\left[F_1 e^{-iS}\right](R+R'\rho)\rho\,d\rho &= L^3\int_0^\infty \Re\left[2i\frac{R^2}{L^2}\frac{\partial}{\partial t}\left(\frac{R}{L}e^{iS}\right)e^{-iS}\right](R+R'\rho)\rho\,d\rho \\
&= -2\int_0^\infty R^3 S_t(R+R'\rho)\rho\,d\rho \\
&= -\frac{2}{L^2}\int_0^\infty R^3(R+R'\rho)\rho\,d\rho - \frac{L_t^2+LL_{tt}}{2}\int_0^\infty R^3(R+R'\rho)\rho^3\,d\rho \\
&= -\frac{1}{L^2}\int_0^\infty R^4\rho\,d\rho + 0 \\
&= -\frac{2N_c}{L^2}
\end{aligned}$$

F_2 :

$$\begin{aligned}
L^3\int_0^\infty \Re\left[F_2 e^{-iS}\right](R+R'\rho)\rho\,d\rho &= L^3\int_0^\infty \Re\left[\nabla_r^2\left(\frac{R}{L}e^{iS}\right)\frac{R^2}{L^2}e^{-iS}\right](R+R'\rho)\rho\,d\rho \\
&= \frac{1}{L^2}\int_0^\infty \left(R''+\frac{1}{\rho}R'-S_\rho^2\right)R^2(R+R'\rho)\rho\,d\rho \\
&= \frac{1}{L^2}\int_0^\infty \left(R-R^3-\frac{L_t^2L^2}{4}\rho^2 R\right)R^2(R+R'\rho)\rho\,d\rho \\
&= \frac{1}{L^2}\left(\int_0^\infty R^3(R+R'\rho)\rho\,d\rho - \int_0^\infty R^5(R+R'\rho)\rho\,d\rho + 0\right) \\
&= \frac{1}{L^2}\left(\frac{1}{2}\int_0^\infty R^4\rho\,d\rho - \frac{2}{3}\int_0^\infty R^6\rho\,d\rho\right) \\
&\equiv \frac{N_c-\frac{2}{3}I_3}{L^2}
\end{aligned}$$

F_3 :

$$\begin{aligned}
L^3\int_0^\infty \Re\left[F_3 e^{-iS}\right](R+R'\rho)\rho\,d\rho &= L^3\int_0^\infty \Re\left[\phi_r^2\phi^* e^{-iS}\right](R+R'\rho)\rho\,d\rho \\
&= \frac{1}{L^2}\int_0^\infty \Re\left[\left(\frac{\partial}{\partial\rho}Re^{iS}\right)^2 Re^{-2iS}\right]R(R+R'\rho)\rho\,d\rho \\
&= \frac{1}{L^2}\int_0^\infty \left((R')^2-S_\rho^2R^2\right)R(R+R'\rho)\rho\,d\rho \\
&= \frac{1}{L^2}\left(\int_0^\infty (RR')^2\rho\,d\rho + \int_0^\infty R(R')^3\rho^2\,d\rho\right) \\
&\equiv \frac{I_4-I_5}{L^2}
\end{aligned}$$

Thus

$$\begin{aligned}\epsilon\frac{\partial}{\partial t}\left(\int_0^\infty hR\rho\,d\rho\right) &= \epsilon\frac{\partial}{\partial t}\left(-\frac{L^3}{2}\int_0^\infty \Re\left[Fe^{-\epsilon iS}\right](R+R'\rho)\rho\,d\rho\right)\\ &= -\epsilon\frac{1}{2}\frac{\partial}{\partial t}\frac{1}{L^2}\left(-2N_c+N_c-\frac{2}{3}I_3+I_4-I_5\right)\\ &= -\epsilon\left(N_c+\frac{2}{3}I_3-I_4+I_5\right)\frac{L_t}{L^3}\end{aligned}$$

$$\epsilon L\int_0^\infty \Im\left[Fe^{iS}\right]R\rho\,d\rho = \epsilon L\int_0^\infty \Im\left[(F_1+F_2+F_3)e^{iS}\right]R\rho\,d\rho$$

F_1 :

$$\begin{aligned}L\int_0^\infty \Im\left[2i\frac{R^2}{L^2}\frac{\partial}{\partial t}\left(\frac{R}{L}e^{iS}\right)e^{-iS}\right]R\rho\,d\rho &= \frac{2}{L}\int_0^\infty R^3\left(\frac{R}{L}\right)_t\rho\,d\rho\\ &= -\frac{2L_t}{L^3}\int_0^\infty R^3(R+R'\rho)\rho\,d\rho\\ &= -\frac{L_t}{L^3}\int_0^\infty R^4\rho\,d\rho\\ &= -2N_c\frac{L_t}{L^3}\end{aligned}$$

F_2 :

$$\begin{aligned}L\int_0^\infty \Im\left[\frac{R^2}{L^2}\nabla_r^2\left(\frac{R}{L}e^{iS}\right)e^{-iS}\right]R\rho\,d\rho &= \frac{1}{L^4}\int_0^\infty R^3\left(\frac{S_\rho}{\rho}R+2S_\rho R'+S_{\rho\rho}R\right)\rho\,d\rho\\ &= \frac{L_t}{L^3}\int_0^\infty R^3(R+R'\rho)\rho\,d\rho\\ &= \frac{L_t}{2L^3}\int_0^\infty R^4\rho\,d\rho\\ &= N_c\frac{L_t}{L^3}\end{aligned}$$

F_3:

$$L\int_0^\infty \Im\left[\left(\frac{R}{Le^{iS}}\right)_r^2 \frac{R}{L}e^{-2iS}\right] R\rho\,d\rho$$

$$\begin{aligned} &= \frac{2}{L^4}\int_0^\infty (RR'S_\rho)R^2\rho\,d\rho \\ &= \frac{L_t}{L^3}\int_0^\infty R^3R'\rho^2\,d\rho \\ &= -N_c\frac{L_t}{L^3} \end{aligned}$$

Whence

$$\begin{aligned} \epsilon L\int_0^\infty \Im\left[Fe^{iS}\right] R\rho\,d\rho &= \epsilon L\int_0^\infty \Im\left[(F_1+F_2+F_3)e^{iS}\right] R\rho\,d\rho \\ &= -\epsilon\frac{L_t}{L^3}(2N_c - N_c + N_c) \\ &= -2\epsilon N_c\frac{L_t}{L^3} \end{aligned}$$

Assembling this monstrosity we have the modulation equation (3.32)

$$\beta_t = \epsilon\frac{I_1}{I_2}\frac{L_t}{L^3} - \frac{N_c}{I_2} - \frac{\gamma}{I_2}\left(\left(1+\frac{L^2L_t^2}{2}\right)J_1 + 2J_3 + (L^2L_t^2-\beta)\left(\frac{1}{4}J_2 + \frac{LL_t}{8}J_4\right)\right)$$

Bibliography

[1] Y. Shen, *The Principles of Nonlinear Optics*, (Wiley, 1984).

[2] A. Hasegawa and F. Tappert. Transmission of stationary nonlinear optical pulses in dispersive dielectric fibers I - anomalous dispersion. *Applied Physics Letters* **23**, 142-144 (1973).

[3] L. Mollenauer, R. Stolen and J. Gordon. Experimental evidence of picosecond pulse narrowing and solitons in optical fibers. *Physical Review Letters* **45**, 1095 (1980).

[4] G. Oppo, M. Brambilla and L. Lugiato. Formation and evolution of roll patterns in optical parametric oscillators. *Physical Review A* **49**, 2028-2032 (1994).

[5] S. Trillo, M. Haelterman and A. Sheppard. Stable topological spatial solitons in optical parametric oscillators. *Optics Letters* **22**, 970-972 (1997).

[6] K. Staliunas and V. Sanchez-Morcillo. Spatial-localized structures in degenerate optical parametric oscillators. *Physical Review A* **57**, 1454-1457 (1998).

[7] S. Trillo and M. Haelterman. Excitation and bistability of self-trapped signal beams in optical parametric oscillators. *Optics Letters* **23**, 1514-1516 (1998).

[8] M. Tlidi, P. Mandel and B. Lefever. Kinetics of localized pattern formation in optical systems.*Physical Review Letters* **81**, 979-982 (1998).

[9] N. Kutz, T. Erneux, S. Trillo and M. Haelterman. Curvature dynamics and stability of topological solitons in the optical parametric oscillator. *J. Optical Society of America B* **16**, 1936-1941 (1999).

[10] P. Mandel. *Theoretical problems in nonlinear cavity optics*, (Cambridge University Press, 1997).

[11] N. Kutz. *Pulse propagation in nonlinear optical fibers using phase-sensitive amplifiers*. PhD thesis, Northwestern University, 1994.

[12] F. Duarte, ed.. *Tunable Lasers Handbook*, (Academic Press, 1995).

[13] K. Promislow and N. Kutz. Bifurcation and asymptotic stability in the large detuning limit of the optical parametric oscillator. *Nonlinearity* **13**, 675-698 (2000)

[14] N. Alexeeva, I Barashenkov and D. Pelinovsky. Dynamics of the parametrically driven NLS solitons beyond the onset of the oscillatory instability. *Nonlinearity* **12**, 103-140 (1999)

[15] I. Barashenkov, M. Bogdan and V. Korobov. Stability diagram of the phase-locked solitons in the parametrically driven, damped nonlinear Schrodinger equation. *Europhysics Letters* **15** 113-118 (1991).

[16] Rasmussen, K., O. Bang and P. Christiansen. Driving and collapse in a nonlinear Schrodinger equation. *Physics Letters A*, **184** 241-244 (1994).

[17] C. Sulem and P Sulem. *The nonlinear Schrodinger equation: Self-focusing and wave collapse*, (Springer 1999).

[18] J. Rasmussen and K. Rypdal. Blow-up in nonlinear Schrodinger equations - I a general review. *Physica Scripta* **33** 481-497 (1986).

[19] G. Papanicolau and G. Fibich. Self-focusing in the perturbed and unperturbed nonlinear Schrodinger equation in critical dimension. *SIAM J. of Applied Math* **60**, 183-240 (2000).

[20] V. Malkin. On the analytical theory for stationary self-focusing of radiation.*Physica D* **64** 251-266 (1993).

[21] E. Ince. *Ordinary Differential Equations.* (Dover, 1926).

[22] R. Peyret and T. Taylor. *Computational methods for fluid flow. Second Edition.* (Springer-Verlag 1985).

[23] G. Strang. On the construction and comparison of difference schemes. *SIAM J. of Numerical Analysis* **5** 506-517 (1968).

[24] W. Huang, Y. Ren and R. Russell. Moving mesh partial differential equation (MMPDEs) based on the equidistribution principle. *SIAM J. Numerical Analysis* **31** 279-290 (1994).

[25] C. Budd, W. Huang and R. Russell. Moving mesh methods for problems with blow-up. *SIAM J. Scientific Computing* **17** 305-327 (1996).

[26] C. Budd, S. Chen and R. Russell. New self-similar solutions of the nonlinear Schrodinger equation with moving mesh computations. *J. Computational Physics* **152** 756-789 (1999).